

The limits of Navier-Stokes theory and kinetic extensions for describing small-scale gaseous hydrodynamics

Nicolas G. Hadjiconstantinou^{a)}

Department of Mechanical Engineering, Massachusetts Institute of Technology,
Cambridge, Massachusetts 02139

(Received 28 June 2006; accepted 1 September 2006; published online 27 November 2006)

This paper reviews basic results and recent developments in the field of small-scale gaseous hydrodynamics which has received significant attention in connection with small-scale science and technology. We focus on the modeling challenges arising from the breakdown of the Navier-Stokes description, observed when characteristic lengthscales become of the order of, or smaller than, the molecular mean free path. We discuss both theoretical results and numerical methods development. Examples of the former include the limit of applicability of the Navier-Stokes constitutive laws, the concept of second-order slip and the appropriate form of such a model, and how to reconcile experimental measurements of slipping flows with theory. We also review a number of recently developed theoretical descriptions of canonical nanoscale flows of engineering interest. On the simulation front, we review recent progress in characterizing the accuracy of the prevalent Boltzmann simulation method known as direct simulation Monte Carlo. We also present recent variance reduction ideas which address the prohibitive cost associated with the statistical sampling of macroscopic properties in low-speed flows. © 2006 American Institute of Physics.

[DOI: [10.1063/1.2393436](https://doi.org/10.1063/1.2393436)]

I. INTRODUCTION

A. Overview

Small-scale, atmospheric pressure, internal gaseous flows have received significant attention in recent years in connection with microscale and nanoscale science and technology.^{1,2} In addition to applications of practical interest, small-scale gaseous hydrodynamics continues to attract significant attention due to the number of scientific challenges it poses.

In this paper we discuss some of the *recent* progress in modeling small-scale *internal* gaseous flows of *engineering interest* in which extensions or alternatives to the Navier-Stokes description are required. In small-scale flows, the Navier-Stokes description is expected to fail^{2,3} when the characteristic hydrodynamic lengthscale approaches the fluid “internal lengthscale;” in dilute gases this scale is associated with the molecular mean free path, the average distance traveled between intermolecular collisions. Until recently, and with the exception of the classical shear, pressure-driven, and thermal-creep-driven duct flows, very few flows of engineering interest have been theoretically characterized, primarily because previous efforts had focused on external, high-speed flows associated with flight in the upper atmosphere. Gaining a fundamental understanding in this new (low-speed) regime is important for facilitating the design of small-scale devices but also for educational purposes. For this reason, particular emphasis will be given here to basic theoretical results for

monoatomic gases, which can facilitate a fundamental understanding of the flow physics.

B. Background

In the small-scale, low-speed flows of interest here, the failure of the Navier-Stokes description can be quantified by the Knudsen number, $Kn = \lambda/H$, where λ is the molecular mean free path and H is the characteristic hydrodynamic lengthscale. The Navier-Stokes description [in the interest of simplicity, limiting cases of this description (e.g., Stokes flow) will not be denoted separately but will be understood to apply under the appropriate conditions] corresponds to the collision-dominated transport limit of small Knudsen number ($Kn \ll 1$). More specifically, in the presence of hydrodynamic gradients in a homogeneous gas over lengthscales characterized by $Kn \ll 1$, the Chapman-Enskog^{4,5} (or Grad-Hilbert;⁶ see Ref. 7 for a critical comparison) expansion procedure can be applied to the governing kinetic (Boltzmann) equation (with Kn as a small parameter) to show that the gas response can be described by linear-gradient constitutive relations which lead to the Navier-Stokes description.^{4,5} Close to the system boundaries, however, the inhomogeneity introduced by the former results in kinetic effects that cannot be captured by the Navier-Stokes description.

Although kinetic effects are always present adjacent to system boundaries (in the presence of nonequilibrium), in the $Kn \ll 1$ limit the former remain localized to thin layers (thickness of order λ) known as Knudsen layers. Analysis of the governing kinetic (Boltzmann) equation shows⁸ that the inhomogeneity induced by the wall presence may be accounted for by a boundary-layer-type theory in which the Navier-Stokes description, albeit subject to slip boundary

^{a)}This paper is based on the invited talk presented by the author at the 58th Annual American Physical Society Division of Fluid Dynamics Meeting, which was held 20–22 November 2005 in Chicago, IL.

conditions, is formally the *outer*, collision-dominated, solution. The inner description, which amounts to a Knudsen layer correction to the flowfield, will be discussed further in Secs. II A and II C 1. In other words, for small Knudsen numbers, kinetic effects at the walls manifest themselves, at the Navier-Stokes description level, in the form of “apparent” hydrodynamic property slip/jump at the boundaries which can be captured by slip-flow boundary conditions (see Sec. II A). For $\text{Kn} \leq 0.1$ a first-order asymptotic theory is sufficiently accurate, especially for practical purposes. For this reason, the regime $\text{Kn} \leq 0.1$ is known as slip flow. It is noteworthy that (for $\text{Kn} \ll 1$) Knudsen layers are present irrespective of the characteristic system lengthscale, H ; however, as Kn decreases, their effect becomes less pronounced, as one would expect, to the extent that in the limit $\text{Kn} \lll 1$ their effect is, for all practical purposes, negligible and the classical no-slip boundary condition becomes an excellent approximation.

When the Knudsen number becomes appreciable ($\text{Kn} \geq 0.1$), one expects kinetic effects to be important in a large part of the domain and the Navier-Stokes description to fail. When the Knudsen number is large ($\text{Kn} \rightarrow \infty$), the rate of intermolecular collisions is very small compared to the rate of molecule-wall collisions. As a result, transport at high Knudsen numbers is ballistic. Ballistic transport is typically assumed to take place for $\text{Kn} \geq 10$. The regime $0.1 \leq \text{Kn} \leq 10$ is known as the transition regime, and is typically the most challenging to model. In this regime, nonlocal transport is important while collisions between molecules are not negligible.

C. Kinetic description

Gaseous hydrodynamics beyond Navier-Stokes can be captured using a kinetic description. Under the assumption of a dilute gas (air at atmospheric pressure satisfies the dilute-gas criteria⁹), a kinetic description characterizes the state of the gas in terms of the single-particle distribution function $f = f(\mathbf{x}, \mathbf{c}, t)$, which is proportional to the probability of finding a particle at a location \mathbf{x} with velocity \mathbf{c} at time t (Ref. 4). Within this description, connection to hydrodynamics is made through the moments of f . For example, the gas density is given by

$$\rho(\mathbf{x}, t) = \int_{\text{allc}} m f d\mathbf{c}, \quad (1)$$

while the gas flow velocity is given by

$$\mathbf{u}(\mathbf{x}, t) = \frac{1}{\rho(\mathbf{x}, t)} \int_{\text{allc}} m \mathbf{c} f d\mathbf{c}. \quad (2)$$

Here m is the molecular mass; $n = \rho/m$ is the gas number density. The gas pressure and temperature will be denoted $P = P(\mathbf{x}, t)$ and $T = T(\mathbf{x}, t)$, respectively, and are given by higher moments of f (Ref. 4).

The evolution of the distribution function is governed by the Boltzmann equation^{7,9}

$$\frac{\partial f}{\partial t} + \mathbf{c} \cdot \frac{\partial f}{\partial \mathbf{x}} + \mathbf{a} \cdot \frac{\partial f}{\partial \mathbf{c}} = \left[\frac{df}{dt} \right]_{\text{coll}}, \quad (3)$$

$$\left[\frac{df}{dt} \right]_{\text{coll}} = \int \int (f' f'_1 - f f_1) g \psi d^2 \Omega d^3 \mathbf{c}_1.$$

Here, $f_1 \equiv f(\mathbf{x}, \mathbf{c}_1, t)$, $f' \equiv f(\mathbf{x}, \mathbf{c}', t)$, $f'_1 \equiv f(\mathbf{x}, \mathbf{c}'_1, t)$, where a prime indicates postcollision velocities. (Postcollision velocities depend on the precollision velocities and the scattering solid angle Ω .) Additionally, $g = |\mathbf{c} - \mathbf{c}_1|$ is the relative precollision speed, ψ is the collision cross section, and \mathbf{a} is the acceleration due to body forces acting on a molecule.

The Boltzmann equation describes a balance between phase-space advection [left-hand side (LHS)] and collisions [right-hand side (RHS)]. The RHS of the Boltzmann equation is typically referred to as the collision integral and contributes significantly to the intransigence of this equation. This led Bhatnagar *et al.*^{10,4} to propose a model equation, known now as the BGK model, which significantly simplifies the mathematics by replacing the collision integral with the simple relaxation model, namely $-(f - f_0)/\tau$; here, f_0 is a Maxwellian distribution at the *local* velocity and temperature and τ is an inverse collision frequency that *does not* depend on the molecular velocity. The value of the collision frequency is usually chosen to match the viscosity of the modeled gas. The BGK model has proven itself as a useful *qualitative* model, because it retains most qualitative features of the Boltzmann equation. One of its major disadvantages is that it predicts a Prandtl number (Pr) of 1 (Refs. 4 and 7), rather than a value close to $2/3$ appropriate for a monoatomic gas; this means that the BGK model cannot match the viscosity and the thermal conductivity of a real gas at the same time, and thus flow calculations involving heat transfer need to be interpreted with great care.

The most prevalent solution method for Eq. (3) is a stochastic particle *simulation* method known as direct simulation Monte Carlo (DSMC). Comprehensive descriptions of this method can be found in Ref. 11 or the monograph by the inventor of this method, Bird;⁹ a brief description is given in Sec. III A. The majority of theoretical developments presented here use DSMC for verification purposes. In some cases, however, DSMC provides the only solution available to the problem of interest.

In the interest of simplicity, unless otherwise stated, the theoretical results and DSMC simulations will be using the hard-sphere (HS) model ($\psi = d^2/4$, where d is the hard-sphere diameter).⁹ The hard-sphere model provides reasonably accurate models of rarefied gas flows,⁷ and for the purposes of this discussion it provides a good compromise between simplicity and realistic modeling. The mean free path of a hard-sphere gas is given by

$$\lambda = \frac{1}{\sqrt{2} \pi n d^2}, \quad (4)$$

while the first-order approximations to the viscosity and thermal conductivity of the hard-sphere gas within the Chapman-Enskog theory are given by

$$\mu = \frac{5}{16d^2} \sqrt{\frac{mk_b T}{\pi}} \quad (5)$$

and

$$\kappa = \frac{75k_b}{64d^2} \sqrt{\frac{k_b T}{m\pi}}, \quad (6)$$

respectively.⁵ Here, T is the gas temperature, k_b is Boltzmann's constant. The above rational approximations to the transport coefficients are typically preferred over the more accurate "infinite-order" expressions from which they only differ by approximately 2% (Ref. 5). One of the disadvantages of the hard-sphere model is that it predicts transport coefficients which are proportional to $T^{0.5}$, whereas real gases exhibit a slightly higher exponent of approximately $T^{0.7}$. To remedy this, collision models with more complex collision cross sections have been proposed;⁹ one example is the variable hard-sphere (VHS) model in which the collision cross section is a function of the relative velocity of the colliding molecules. The discussion in this paper can easily be extended to these modified collision models.

D. Further remarks

Gaseous flows beyond the Navier-Stokes regime ($\text{Kn} \geq 0.1$) are frequently referred to as rarefied, most likely due to historical reasons, viz the rarefied gas dynamics literature,^{9,12} where deviation from Navier-Stokes was extensively studied in the context of high altitude aerodynamics. Flows for which the Navier-Stokes description breaks down are also frequently referred to as "noncontinuum;" this terminology is very common within the rarefied gas dynamics⁹ and now the microelectromechanical systems (MEMS) literature, and may, unfortunately, lead to confusion in a mechanics setting where the expression "noncontinuum" will most likely be associated with a breakdown of the continuum assumption. One may surmise that use of the term "noncontinuum" derives from the view that because the continuum approach culminates in the Navier-Stokes equations, when the latter fails, the continuum approach fails, without this necessarily implying failure of the continuum assumption. We would thus like to emphasize that for a large class of the problems of practical interest, including the ones discussed here, hydrodynamic fields and the associated conservation laws remain well defined. The view taken in this paper is the one typically adopted within the rarefied gas dynamics community and described in Ref. 4: conservation laws for mass, momentum, and energy follow naturally from moments of the Boltzmann equation. The implied averaging procedure can be performed using an ensemble of realizations (with no restrictions on space or time averaging intervals), thus leading to a meaningful description in terms of said conservation laws (i.e., both in the presence and absence of Navier-Stokes closures), for quite a wide range of conditions, including very small lengthscales and time scales.

II. FLOW PHYSICS

In this section we will review theoretical results focusing on the physics of problems of engineering interest; both re-

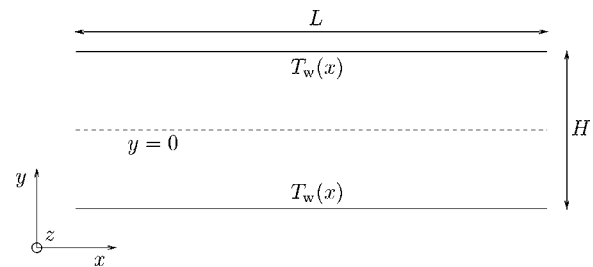


FIG. 1. Two-dimensional channel geometry and nomenclature.

cent and basic fundamental results will be discussed. One of the basic geometries that we will visit frequently is a two-dimensional channel such as the one shown in Fig. 1. The two-dimensional channel geometry has been widely studied in the context of small-scale flows due to its direct relevance to typical small-scale applications, but also due to its simplicity, which enables investigations aimed at the physics of transport at small scales.

A. First-order slip-flow theory

When the Knudsen number is small, solution of the linearized Boltzmann equation can be obtained using asymptotic approaches.^{6,8} By taking advantage of the fact that for $\text{Kn} \leq 0.1$ kinetic effects are limited to the vicinity of the walls, one can obtain solutions of the linearized Boltzmann equation by superposing a Navier-Stokes solution with a kinetic boundary (Knudsen) layer correction, where the latter is significant only up to distances of the order of one mean free path from the wall (see Fig. 2).

The matching procedure between inner and outer solutions leads to "effective" boundary conditions for the Navier-Stokes description, known as slip-flow relations. Using these boundary conditions, the Navier-Stokes description is able to capture the (bulk) flowfield *away from the walls*. These relations, to first order in Kn , can be written as follows:

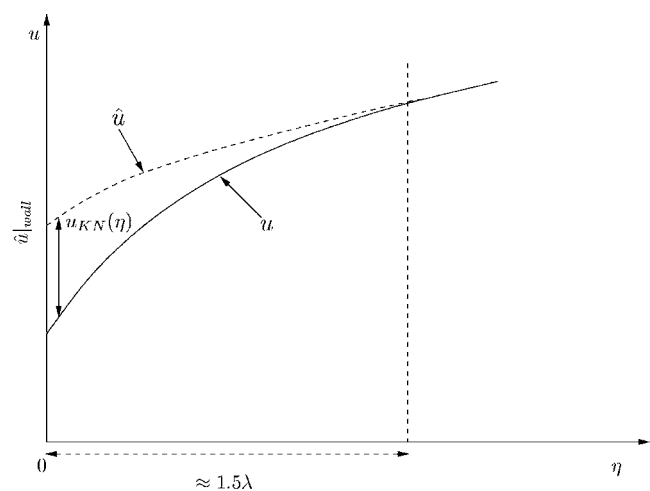


FIG. 2. Schematic of the Knudsen layer in the vicinity of the wall ($\eta=0$).

$$u_s^{\text{NS}}|_{\text{wall}} - U_s = \alpha \lambda_v \left. \frac{du_s^{\text{NS}}}{d\eta} \right|_{\text{wall}} + \phi \lambda_v \sqrt{\frac{2k_b}{\pi m T}} \left. \frac{dT^{\text{NS}}}{ds} \right|_{\text{wall}}. \quad (7)$$

Here, s is the coordinate tangent to the wall, η is the coordinate normal to the wall and pointing into the gas, and U denotes wall velocity. The superscript NS is used to differentiate between the linearized Boltzmann equation solution (no superscript), which is the “true” flowfield, and the Navier-Stokes (slip-flow) approximation to this solution; as stated above, the two are related through the superposition of a Knudsen layer correction, e.g., $u_s = u_s^{\text{NS}} + u_s^{\text{Kn}}$, $T = T^{\text{NS}} + T^{\text{Kn}}$, ..., with these corrections decaying fast away from the walls, i.e., $u_s^{\text{Kn}}, T^{\text{Kn}} \rightarrow 0$ as $\eta/\lambda_v \rightarrow \infty$.

Also, λ_v is a viscosity-based mean free path defined by

$$\lambda_v = \frac{\mu}{P} \sqrt{\frac{\pi R T}{2}}. \quad (8)$$

This definition is very useful for molecular models without a well-defined range of interaction where a mean free path is difficult to define.⁷ Note that this definition is such that $\lambda_v = \lambda = (\sqrt{2} \pi n d^2)^{-1}$ for the hard-sphere gas. The hard-sphere results presented below have been developed using $\lambda_v \equiv (\sqrt{2} \pi n d^2)^{-1}$; the slight numerical difference [$\lambda_v \approx (\sqrt{2} \pi n d^2)^{-1}$] observed when one uses (5) into (8) is due to the use of a rational form for (8) in the interests of simplicity.

The temperature jump at the wall is given by the following analogous expression:

$$\hat{T}|_{\text{wall}} - T_w = \zeta \frac{2\gamma}{\gamma + 1} \frac{\lambda_v}{Pr} \left. \frac{dT}{d\eta} \right|_{\text{wall}}, \quad (9)$$

where γ is the ratio of specific heats.

The coefficients α , ϕ , and ζ are determined by matching the outer and inner descriptions within the asymptotic solution. Maxwell was able to *estimate* these coefficients *without* solving the Boltzmann equation using insightful physical arguments; he found

$$\alpha = \frac{2 - \sigma}{\sigma}, \quad \phi = 0.75, \quad (10)$$

where σ is the accommodation coefficient which parametrizes the gas-wall-surface interaction and denotes the fraction of diffusely reflected molecules ($1 - \sigma$ being the fraction of molecules reflected specularly) at the surface. In a similar fashion, ζ was estimated by von Smoluchowski¹³ to equal

$$\zeta = \frac{2 - \sigma}{\sigma}. \quad (11)$$

The amount of slip at the surface is clearly a strong function of the accommodation coefficient. Our discussion will be limited to the interpretation given above—known as Maxwell’s gas-surface interaction model¹⁴—primarily because the majority of theoretical results have been obtained using this model. A number of more complex models exist, typically relying on more than one accommodation coefficient; for example, the use of separate momentum and en-

ergy accommodation coefficients is common.^{2,13} Scattering kernels based on more than one accommodation coefficient have been developed,^{7,15} but theoretical results on the behavior of slip coefficients are very few and scattered.⁷ A discussion of accommodation coefficients can be found in Ref. 14.

Solutions of the Boltzmann equation for the slip coefficients were originally obtained for the significantly simpler BGK model. Early work by Cercignani,^{7,16} and recent results for the hard-sphere gas, show that *the first-order coefficients* are fairly insensitive to the gas model (e.g., hard sphere, BGK). Thus, although hard-sphere results are more realistic, in our discussion below we will also include BGK results, especially since in some cases they are the only ones available.

Solutions of the Boltzmann equation have mostly focused on the fully accommodating case ($\sigma = 1$), primarily because for most “engineering surfaces” of practical interest $\sigma \approx 1$ (Refs. 9 and 17). In this limit, it is known that $\alpha(\text{BGK}, \sigma = 1) = 1.1466$, $\phi(\text{BGK}, \sigma = 1) = 1.149$, $\zeta(\text{BGK}, \sigma = 1) \approx 1.168$. [When reporting BGK results for ϕ and ζ , a number of authors introduce a correction for the fact that for the BGK model $Pr = 1$ rather than the more realistic (for a monoatomic gas) value of $2/3$. This correction amounts to multiplying these coefficients by $3/2$ (as a result of enhancing the collision frequency by the same amount in order to match the value of thermal conductivity).⁷ This correction *has been applied* throughout this paper.] On the other hand, $\alpha(\text{HS}, \sigma = 1) = 1.11$, $\phi(\text{HS}, \sigma = 1) = 1.015$, $\zeta(\text{HS}, \sigma = 1) = 1.13$ (Ref. 18), verifying that *first-order slip coefficients* are fairly insensitive to the gas model and that Maxwell’s estimate is approximately 10%–15% in error in the diffuse reflection ($\sigma = 1$) limit. This discrepancy has implications in the interpretation of experimental results and will be discussed below. In the limit $\sigma \rightarrow 0$, $\alpha(\text{BGK}) \rightarrow 2/\sigma$ (Ref. 19), in agreement with Maxwell’s approximate solution.

Very few results exist for intermediate values of accommodation coefficients. Loyalka²⁰ used a variational approach to show that for the BGK model a linear interpolation between the $\sigma = 1$ and $\sigma \rightarrow 0$ limits provides reasonable accuracy, i.e.,

$$\begin{aligned} \alpha(\text{BGK}, \sigma) &\approx \frac{2 - \sigma}{\sigma} (1 + [\alpha(\text{BGK}, \sigma = 1) - 1] \sigma) \\ &= \frac{2 - \sigma}{\sigma} (1 + 0.1466 \sigma). \end{aligned} \quad (12)$$

In the case of the temperature jump coefficient, Loyalka²⁰ finds that similar interpolation between the fully accommodating and specular reflection limits may be applied for intermediate values of σ . For the thermal creep slip coefficient, Loyalka and Cipolla find¹⁴

$$\phi(\text{BGK}, \sigma) = 0.75 + 0.399 \sigma. \quad (13)$$

Discussion:

(1) Slip-flow theory naturally reduces to no-slip boundary conditions in the limit $\text{Kn} \lll 1$. This can be easily seen by nondimensionalizing η in Eqs. (7) and (9) using the characteristic lengthscale H .

- (2) The above slip-flow relations are formally valid for steady flows. Comparison of transient slip-flow solutions to solutions of the Boltzmann equation suggest that the above slip-flow relations remain accurate for time-dependent flows, provided the latter are evolving at sufficiently long time scales. One may expect that this effectively “quasistatic” behavior would be observed when the hydrodynamic evolution time scale is long compared to the molecular collision time that characterizes the evolution of kinetic effects at the wall. This is verified by theoretical treatments of the Boltzmann equation, at least in the BGK approximation,²¹ where slip-flow relations equivalent (at least formally) to the above are obtained by assuming that the evolution time scale is long compared to the molecular collision time $\tau_c = \lambda/\bar{c}$; here $\bar{c} = \sqrt{8k_b T/(\pi m)}$ is the mean thermal speed. As shown and discussed further in Sec. II C 1, our results obtained using the second-order slip model of that section confirm that.
- (3) Corrections to the above slip relations due to wall curvature are formally of second order in the Knudsen number⁷ and are given in Ref. 6.
- (4) First-order Knudsen layer corrections for the most common state variables and their fluxes are tabulated in Ref. 6 for the BGK and HS models; the lack of analytical descriptions is the primary reason for their neglect in engineering analysis. In Sec. II C 1 we will discuss the Knudsen layer correction for the tangential flow velocity; we will illustrate that its contribution to the average flow velocity is of order Kn^2 (Ref. 22), and show how it can be incorporated into a second-order slip model.
- (5) Conveniently, the first-order Knudsen layer correction for the stress tensor is zero in isothermal flow; this means that within slip-flow theory the stress field is given by the Navier-Stokes solution (no modification to the Navier-Stokes constitutive relation is required or allowed; in fact, this is one of the basic premises and undoubtedly one of the great advantages of slip-flow theory). In a similar fashion, the first-order Knudsen layer correction to the heat flux in the direction normal to the wall in the presence of a temperature gradient in the same direction is zero.
- (6) In addition to the experimental difficulties associated with accurate measurement of accommodation coefficients, theoretical difficulties make this an even harder task. One such difficulty is the uncertainty associated with the gas-surface interaction model; although Maxwell’s accommodation model is frequently used in theoretical studies, experimental results have not reached a consensus on whether it accurately describes gas-surface interaction, or whether a more complex model is required. This uncertainty is compounded by the fact that experimental results are typically compared to Maxwell’s estimates for the slip coefficients [Eqs. (10) and (11)], which can lead to errors in accommodation coefficients (of the order of 5%). From a number of experimental studies conducted to date (see, for example, Refs. 2, 9, 17, 23, and 25), it appears that for “engineering surfaces” the accommodation coefficient is close to 1.

Recent experiments using air on silicon find accommodation coefficients in the range 0.85–0.95 (Ref. 2); for these measurements, the actual accommodation coefficients are *probably* even closer to 1 for two reasons:

- (a) Experimental results are typically interpreted using Eqs. (10) and (11), which underestimate the value of the slip coefficient and would thus lead to lower estimates of σ .
 - (b) A number of experimental studies extend to $\text{Kn} > 0.1$ while still using first-order slip-flow relations. In pressure-driven flows, second-order slip effects increase the amount of slip present (see Sec. II C 1). Neglecting second-order slip effects would again lead to lower estimates of σ .
- (7) Thermal creep phenomena extend beyond the slip-flow regime; thermal creep flow for all Knudsen numbers for the hard-sphere model has been characterized in Ref. 18.

Unless otherwise stated, in what follows we will assume that $\sigma=1$ and thus $\alpha=1.11$, $\phi=1.015$, and $\zeta=1.13$.

B. Isothermal pressure-driven flows in two-dimensional channels

Isothermal pressure-driven flow in two-dimensional ducts for $\text{Kn} > 0.1$ was originally studied by Knudsen.²⁶ He studied the flow through capillaries and showed the existence of a minimum in the flow rate when the latter is normalized by the pressure difference driving the flow and plotted against the average pressure in the channel (inverse Knudsen number);² this minimum cannot be predicted by the Navier-Stokes description. Following Knudsen’s discovery, a theoretical description of this phenomenon remained a significant challenge for a number of years.

Following the development of semianalytical solutions of simple models of the Boltzmann equation (e.g., BGK),²⁷ numerical solutions of the linearized Boltzmann equation for the more realistic hard-sphere gas for various two-dimensional geometries were finally developed.¹⁸ For two-dimensional channels (as in Fig. 1) the gas response for arbitrary Knudsen numbers is typically expressed in kinetic terms through the following expression:

$$\dot{Q} = u_b H = - \frac{1}{P} \frac{dP}{dx} H^2 \sqrt{\frac{RT}{2}} \bar{Q}, \quad (14)$$

where \dot{Q} is the volumetric flow rate per unit depth, u_b is the bulk (average over the channel width) velocity, $R=k_b/m$ is the gas constant, and $\bar{Q}=\bar{Q}(\text{Kn})$ is a proportionality coefficient whose dependence on Kn is shown in Fig. 3. Similarly defined \bar{Q} parameters have now been tabulated for a variety of two-dimensional duct geometries.² Note that the linearized treatment assumes a constant pressure gradient; in other words these solutions do not include the effects of stream-wise acceleration due to the gas compressibility.

As shown in Fig. 3, $\bar{Q}(\text{Kn})$ for a two-dimensional channel in the transition regime varies slowly about its minimum value occurring at $\text{Kn} \approx 1$. Numerical solutions, such as lin-

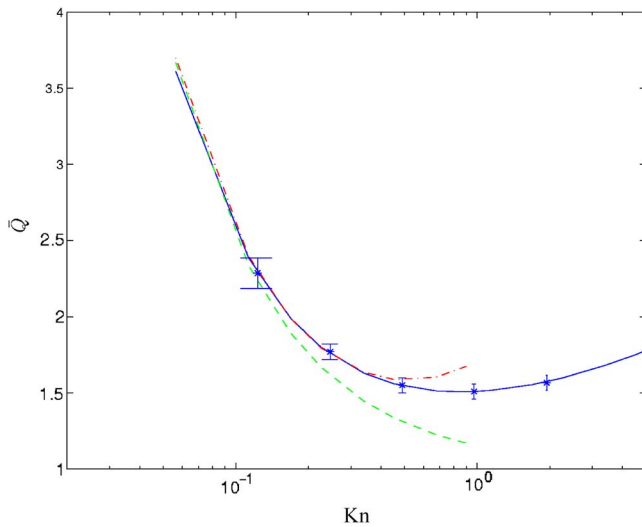


FIG. 3. (Color online) Nondimensional flow rate as a function of the Knudsen number for fully developed pressure-driven flow. The solid line denotes \bar{Q} as determined by solution of the linearized Boltzmann equation for a hard-sphere gas (Ref. 18), and the dash-dotted line denotes the second-order slip model discussed in Sec. II C 1. The stars denote DSMC simulation results, and the dashed line a first-order slip model.

earized solutions of the Boltzmann equation for hard spheres^{7,18,28} and molecular simulations,²⁸ have been shown to be in good agreement with experiments.^{7,28}

C. Second-order velocity slip

Slip-flow solutions to a variety of problems of practical interest suggest that slip-flow theory is remarkably robust, in the sense that it continues to be reasonably accurate, at least in a qualitative sense, well beyond its expected limits of applicability ($\text{Kn} \approx 0.1$); examples in this paper include the pressure-driven flow of Sec. II B and the convective heat-transfer problem of Sec. II G. Robust slip-flow models will always be preferable to alternatives such as molecular simulations or solutions of the Boltzmann equation, since the difficulty associated with solving the Navier-Stokes equations is negligible compared with the cost of these alternative methods. For this reason, a variety of researchers^{22,24,25,28–30} have attempted to develop or evaluate slip models that can be used beyond $\text{Kn} \approx 0.1$. A review of a number of these approaches can be found in Ref. 2. In this paper we will discuss approaches which fall within the rigorous framework of asymptotic analysis of the Boltzmann equation.

Although the general structure of slip-flow relations up to second order in Kn has been known for some time,^{8,31} and the second-order coefficient for one-dimensional, isothermal flow for the BGK model was calculated by Cercignani²² as early as 1964, the calculation of other second-order slip coefficients has proven to be a significantly harder task. Second-order slip coefficients for the BGK model have eventually been calculated;^{6,7,22} these, however, unlike the first-order slip coefficients, are not necessarily approximately equal to the corresponding coefficients of the more realistic hard-sphere model. This has been one of the main reasons for the lack of interest in second-order slip-flow theory, since

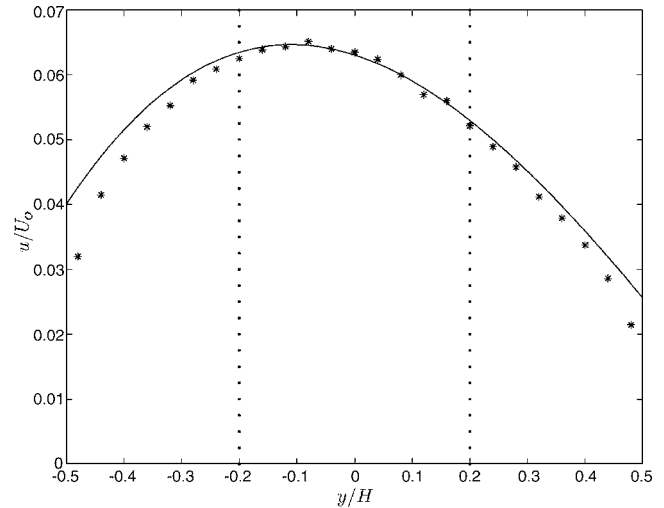


FIG. 4. Snapshot of flow velocity in an oscillatory Couette flow at $\text{Kn}=0.2$. The stars represent the DSMC solution (u) and the solid line the Navier-Stokes approximation to this solution (u^{NS}). The vertical dotted lines illustrate the approximate thickness of the Knudsen layers. U_o is the wall-velocity amplitude.

agreement with experiments and solutions of the Boltzmann equation (e.g., DSMC simulations) could not be achieved using the BGK theory. Another reason for the lack of interest in the second-order slip-flow theory is the special care needed in interpreting slip-flow solutions and comparing those to numerical solutions of the Boltzmann equation or experimental data due to the presence of Knudsen layers in the flow. This is illustrated in Fig. 4, which shows the extent of Knudsen layers in a one-dimensional flow at $\text{Kn}=0.2$ by comparing the Boltzmann solution ($u=u^{\text{NS}}+u^{\text{KN}}$) to the Navier-Stokes solution u^{NS} (obtained using the second-order slip model to be introduced in the next section); this figure clearly illustrates that, at this Knudsen number, Knudsen layers from both walls penetrate approximately 60% of the physical domain. This means that the effective width of the Knudsen layer is approximately $1.5\lambda_v$ (this will also be discussed in more detail below), and thus for $\text{Kn} \geq 0.3$ direct comparison between the Navier-Stokes and the true flowfield is impossible.

1. A second-order slip model for the hard-sphere gas

To address this deficiency, the author has developed³² a second-order slip model for the hard-sphere gas. According to this model, for one-dimensional (variations only in η direction), fully accommodating ($\sigma=1$) flows, the second-order slip is given by

$$u_s^{\text{NS}}|_{\text{wall}} - U_s = \alpha \lambda_v \left. \frac{\partial u_s^{\text{NS}}}{\partial \eta} \right|_{\text{wall}} - \beta \lambda_v^2 \left. \frac{\partial^2 u_s^{\text{NS}}}{\partial \eta^2} \right|_{\text{wall}}, \quad (15)$$

where $\beta=0.61$ is the second-order slip coefficient ($\alpha=1.11$). Validation of this model for a variety of flows shows excellent agreement up to $\text{Kn} \approx 0.4$ (provided the effect of the Knudsen layers is properly accounted for).

The first-order Knudsen layer correction in the tangential flow velocity $u_s^{\text{KN}}(\eta)$ can be written as

$$u_s^{KN}(\eta/\lambda_v) = -\lambda_v \left. \frac{du_s^{NS}}{d\eta} \right|_{\text{wall}} I_1(\eta/\lambda_v), \tag{16}$$

where $I_1(\eta/\lambda_v)$ is a positive function that decays to zero for $\eta/\lambda_v \gg 1$; it has been numerically calculated for both the BGK (Ref. 7) and HS gas.³³ The implication of this relation is that the Knudsen layer correction is parametrized by the Navier-Stokes solution. In other words, despite the fact that the underlying distribution in the Knudsen layer differs from the Chapman-Enskog solution, this correction becomes a functional of, and is thus effectively determined by, the local Navier-Stokes solution (after a short transient of the order of the collision time; the length of time over which this relaxation takes place has implications in the validity of slip-flow theory in transient flows, and is discussed in Sec. II A and below). Tabulated values show that $u_s^{KN}(\eta/\lambda_v)$ decays to approximately 3% of its maximum value [$u_s^{KN}(\eta/\lambda_v=0)$] at $\eta = 1.5\lambda_v$; we will refer to this distance as the effective width of the Knudsen layer.

Due to the lack of an analytical description for $u_s^{KN}(\eta/\lambda_v)$, the contribution of the Knudsen layer can be most conveniently accounted for in an average sense, i.e., when calculating averages over the domain. In a one-dimensional geometry such as that of Fig. 1, the average (bulk) flow velocity is given by

$$u_b = \frac{1}{H} \int_{-H/2}^{H/2} u_x dy = \frac{1}{H} \int_{-H/2}^{H/2} [u_x^{NS} + u_x^{KN}] dy. \tag{17}$$

Recalling that $\lambda_v/H \ll 1$ we define $\delta = \int_0^\infty I_1(\eta/\lambda_v) d(\eta/\lambda_v)$ to obtain

$$\begin{aligned} u_b &= \frac{1}{H} \int_{-H/2}^{H/2} u_x^{NS} dy - \frac{\delta \lambda_v^2}{H} \left. \frac{du_x^{NS}}{dy} \right|_{-H/2} + \frac{\delta \lambda_v^2}{H} \left. \frac{du_x^{NS}}{dy} \right|_{H/2} \\ &= \frac{1}{H} \int_{-H/2}^{H/2} \left[u_x^{NS} + \delta \lambda_v^2 \frac{\partial^2 u_x^{NS}}{\partial y^2} \right] dy, \end{aligned} \tag{18}$$

where $\delta=0.296$ (Ref. 32). In other words, the contribution of the Knudsen layer to the average flow velocity is $O(\text{Kn}^2)$.

The above value for δ was obtained by using the fact that the Knudsen layer function I_1 for the hard-sphere gas is very similar to the BGK Knudsen layer function whose integral is known exactly. (A slightly more precise value for δ could have been obtained if one integrated the hard-sphere Knudsen layer function; unfortunately, this value can only be obtained approximately by numerically integrating the tabulated solution for this function.)

While the contribution of the Knudsen layer can always be found by a Boltzmann equation analysis, the value of Eq. (18) lies in the fact that it relates this contribution to the Navier-Stokes solution and thus it requires no solution of the Boltzmann equation. This correction makes comparison to Boltzmann equation solutions possible when Knudsen layers occupy a large fraction of the domain; additionally, it makes comparison possible with experiments which report average flow rates. In fact, it has already been used to explain recent experimental data: a direct consequence of the above relation is that in Poiseuille-type flows, where $\partial^2 u_x^{NS}/\partial y^2$ is a con-

stant, experimental measurement of the flow rate (mean flow velocity) yields an “effective” second-order slip coefficient $\beta - \delta$ (see also Ref. 32). In other words, while the *average value* of a (Navier-Stokes) Poiseuille profile subject to second-order slip of the form (15) is given by

$$u_b^{NS} = \frac{1}{H} \int_{-H/2}^{H/2} u_x^{NS} dy = -\frac{H^2}{2\mu} \frac{dP}{dx} \left(\frac{1}{6} + \alpha \text{Kn} + 2\beta \text{Kn}^2 \right), \tag{19}$$

the *true* bulk flow speed (as inferred by an experiment measuring the flow rate) is given by Eq. (18), which leads to

$$\begin{aligned} u_b &= \frac{1}{H} \int_{-H/2}^{H/2} \left[u_x^{NS} + \delta \lambda_v^2 \frac{\partial^2 u_x^{NS}}{\partial y^2} \right] dy \\ &= -\frac{H^2}{2\mu} \frac{dP}{dx} \left(\frac{1}{6} + \alpha \text{Kn} + 2\epsilon \text{Kn}^2 \right) \end{aligned} \tag{20}$$

or

$$\begin{aligned} \bar{Q} &= \frac{4}{15\sqrt{\pi}} \frac{1 + 6\alpha \text{Kn} + 12\epsilon \text{Kn}^2}{\text{Kn}} \\ &\approx \frac{\sqrt{\pi} 1 + 6\alpha \text{Kn} + 12\epsilon \text{Kn}^2}{12 \text{Kn}}, \end{aligned} \tag{21}$$

with $\epsilon = \beta - \delta = 0.31$. (The above two expressions for \bar{Q} differ by less than 2%; the difference between them is due to the use of slightly different approximations for the hard-sphere gas viscosity.^{5,22}) As shown in Fig. 3, the above equation captures the flow rate in isothermal pressure-driven flow very accurately up to $\text{Kn} \approx 0.4$. This is also demonstrated in Sec. II E, where the pressure-driven flow rate is used to determine the wave propagation constant in two-dimensional channels (under the long-wavelength approximation).

Most importantly, the above model explains the findings of recent experiments²⁵ on helium and nitrogen flow in small-scale channels; these experiments find the second-order slip coefficient to be approximately 0.25 ± 0.1 . Of course, since the slip coefficient was determined by measuring the *flow rate*, these experiments were in fact determining the effective second-order slip coefficient ϵ , which is in good agreement with the value 0.31 given above.

Discussion:

- (1) The second-order Knudsen layer correction for the hard-sphere model has not been calculated. Its contribution to the mean flow velocity was not required in (18) since it is of higher order.
- (2) The second-order Knudsen layer correction to the stress tensor *in isothermal flow* is zero.⁶ Thus, no modification to the Navier-Stokes constitutive relation is required (allowed) within isothermal slip-flow theory.
- (3) In higher spatial dimensions, additional terms appear in Eqs. (15) and (18). In the case of Eq. (15), these terms also include contributions from the curvature of the boundary. As a result, the “effective” second-order slip coefficient for flow in tubes is different (see experimen-

tal results of Ref. 30, but note that this fact was overlooked in the paper) than the one for two-dimensional channels (ε).

- (4) The assumption of variations only in the normal-to-the-wall direction, inherent in the model described above, is not very restrictive. Approaches based on assumptions of slow variation in the axial direction (x in Fig. 1), such as the widely used locally fully developed assumption or long-wavelength approximation, are expected to yield excellent approximations when appropriately used for two-dimensional problems. This is verified by comparison of solutions of such problems to DSMC simulations (see Sec. II E for example) or experiments (e.g., Ref. 25).
- (5) The linearized conditions ($\text{Ma} \ll 1$) under which the second-order slip framework is derived,^{6,8,31} imply $\text{Re} \ll 1$ since $\text{Ma} \approx \text{ReKn}$ and $\text{Kn} > 0.1$. Here Ma is the Mach number and Re is the Reynolds number, based on the same characteristic lengthscale as Kn .
- (6) It appears that the steady-flow assumption on which this model is based does not significantly limit its applicability. As discussed in Sec. II A, slip-flow theory appears to extend to flows that evolve at time scales that are long compared to the molecular collision time; in fact, our results, some of which will be shown below, suggest that the quasistatic behavior of slip at the wall seems to hold for time scales $\geq 5\tau_c$, which correspond to viscous evolution time scales for lengthscales characterized by $\text{Kn} \leq 0.4$; this restriction on evolution timescale is easily satisfied by the vast majority of practical flows of interest.
- (7) Comparisons with solutions of the Boltzmann equation for a variety of problems^{34–36} show that the above slip model provides reasonably accurate approximations to solutions of the Boltzmann equation up to $\text{Kn} \approx 0.4$ (maximum error at $\text{Kn} \approx 0.4$ is of the order of a few percent for both flow speed and stress). Moreover, it remains qualitatively robust well beyond this Knudsen number. This is rather remarkable for a number of reasons: first, for $\text{Kn} \geq 0.3$ the Knudsen layers, treated within the theory as thin boundary layers at the wall [see, for example, the development of Eq. (18)], merge, leading to kinetic corrections that overlap but apparently may still be superposed. Moreover, although a kinetic correction is required throughout the physical domain for $\text{Kn} \geq 0.3$, it appears that the underlying Navier-Stokes constitutive relation remains robust (the stress field is accurately captured for arbitrary flows with **no adjustable parameters**) up to $\text{Kn} \approx 0.4$ (at $\text{Kn} = 0.4$ the domain width is 2.5λ).

2. Example

To illustrate some of the discussion items above, we present a solution of a one-dimensional model problem. Consider the two-dimensional channel of Fig. 1 in which both channel walls impulsively start to move at time $t=0$ in the x direction with velocity U_x ; this velocity is small compared to the most probable molecular velocity ($\text{Ma} \ll 1$). Figure 5

shows a comparison between second-order-slip-corrected Navier-Stokes solution and DSMC simulations for $\text{Kn} = 0.21$. The top plot shows the flowfield at three different times; the existence of the Knudsen layer, manifested by the difference between the DSMC solution and the Navier-Stokes solution, can be seen clearly. The three snapshots also clearly illustrate how the magnitude of the Knudsen layer correction scales with $\partial u^{\text{NS}} / \partial y|_{\text{wall}}$. The middle plot shows the stress field at the same three times, and demonstrates that no Knudsen layer correction exists close to the wall. The bottom plot shows the bulk flow velocity (u_b) as a function of time: as this plot shows, this quantity can be calculated to excellent accuracy using Eq. (18). This last comparison (as well as a comparison of the stress field) becomes particularly useful as Kn increases to $\text{Kn} \approx 0.3$ and beyond, where the Knudsen layer essentially covers the whole physical domain. This is illustrated in Fig. 6, where a comparison at $\text{Kn} = 0.35$ is shown. The figure verifies that although the Knudsen layers cover the physical domain, the second-order slip remains reasonably accurate in predicting the stress field and bulk flow velocity, especially considering that the comparison takes place for times as low as five collision times. Comparisons at higher Knudsen numbers^{34,35} show that, even though the Knudsen layers have penetrated to the middle of the domain, the slip model remains quantitatively accurate up to $\text{Kn} \approx 0.4$, and qualitatively accurate well beyond that. *In some cases* (see next section) *quantitative* accuracy extends up to $\text{Kn} \approx 1$.

D. Oscillatory shear flows

Oscillatory shear flows (one wall in Fig. 1 oscillates in the x direction with velocity amplitude U_o and frequency ω) are very common in MEMS and are considered to be of “tremendous importance in MEMS devices.”³⁷ A comprehensive simulation study of rarefaction effects on oscillatory shear (Couette) flows was recently conducted by Park *et al.*³⁸

Park *et al.* used an extended first-order slip-flow relation with a number of adjustable coefficients to describe the amount of slip at the wall for all Knudsen numbers, provided the flow was quasistatic (i.e., the Stokes number $S = \sqrt{\omega H^2 / \nu}$ is much smaller than 1). Note that the quasistatic assumption is not at all restrictive in practical applications where the gap size, H , is very small. Also note that in the quasistatic regime, shear flow results in a linear velocity profile (at the Navier-Stokes level of approximation) and thus describing the amount of slip completely characterizes the flowfield.

The oscillatory shear flow problem was used in Refs. 34 and 35 as a validation test problem for the second-order slip model of Sec. II C 1. Excellent agreement with DSMC solutions was found for all S for $\text{Kn} \leq 0.4$ for both the flowfield and the stress field. In fact, for sufficiently low frequencies ($S \leq 1$) the agreement is very good up to $\text{Kn} \approx 1$ (note that for this flow, in the quasistatic regime $S \ll 1$, the second-order slip model reduces to the first-order slip model, which is known to describe the stress very well up to $\text{Kn} \approx 1$). Figure 7 shows a comparison between DSMC solutions and the second-order slip model of Sec. II C 1 for the magnitude of

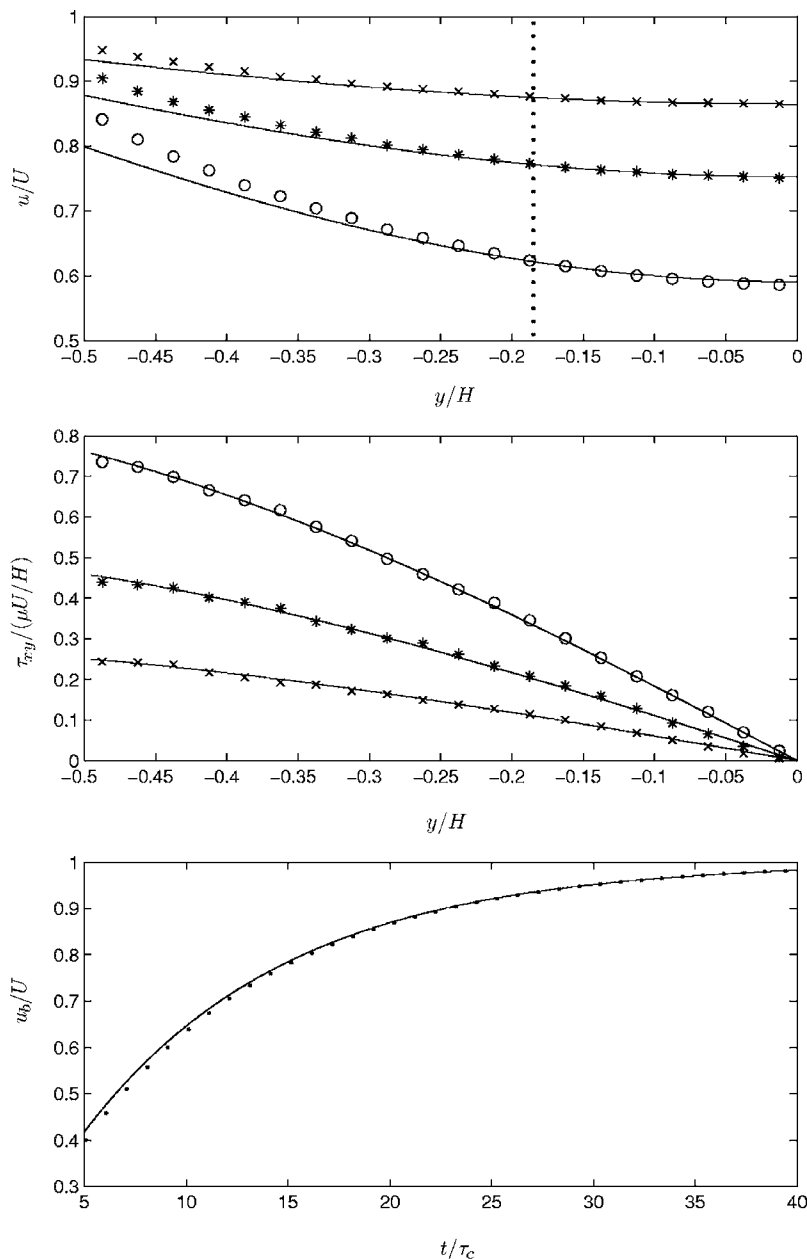


FIG. 5. Comparison between DSMC results (symbols) and second-order-slip-corrected Navier-Stokes solution (lines) for $\text{Kn}=0.21$, for the impulsive start problem described in Sec. II C 1. Due to the problem symmetry about $y=0$, only half domain is shown; the wall is at $y/H=-0.5$. Flowfield and stress plots shown at three times: $11.1\tau_c$ (\circ), $16.2\tau_c$ ($*$), and $22.3\tau_c$ (\times). Top plot: comparison of flow velocities; the Knudsen layer contribution ($u-u^{\text{NS}}$) is visible close to the wall (the vertical dotted line delimits the approximate extent of the Knudsen layer $(-0.5 < y/H \leq -0.185)$). Middle plot: comparison of the shear stress. Bottom plot: comparison of the bulk velocity as a function of time.

the shear stress at the wall. This comparison shows that for $S \leq 1$ the second-order slip model in conjunction with a collisionless model (shown in dashed line) may be used to bridge the transition regime.

The collisionless result of Fig. 7 was given by Park *et al.*, who showed that the velocity and shear stress at the wall are independent of ω and equal to the values of the steady problem. Analytical results for the flowfield and the bounded (ballistic) shear layers appearing at high frequency in the $\text{Kn} \gg 1$ limit—analogue to Stokes layers in the $\text{Kn} \ll 1$ limit—were given by the present author in Ref. 35.

E. Axial wave propagation in small-scale channels

In this section we discuss a theory of axial plane-wave propagation in two-dimensional channels (Fig. 1) for arbitrary Knudsen numbers. The theory is based on the long-wavelength approximation and on the observation that, in the

Navier-Stokes limit, the propagation of disturbances in small-scale channels for most frequencies of practical interest is viscous dominated. The importance of viscosity can be quantified by a narrow channel criterion, $S = \sqrt{\omega H^2 / \nu} \ll 1$. When $S \ll 1$ (whereby the channel is termed narrow) the viscous diffusion length based on the oscillation frequency is much larger than the channel height; viscosity is expected to be dominant and inertial effects will be negligible. This observation has two corollaries; first, since the inertial effects are negligible the flow is governed by the steady equation of motion, that is, the flow is effectively quasisteady.³⁹ Second, since for gases the Prandtl number is of order one, the flow is also isothermal (for a discussion see Ref. 40). This was first realized by Lamb,⁴¹ who used this approach to describe wave propagation in small-scale channels using the Navier-Stokes description. Lamb's prediction for the propagation constant using this theory is identical to the more general theory of

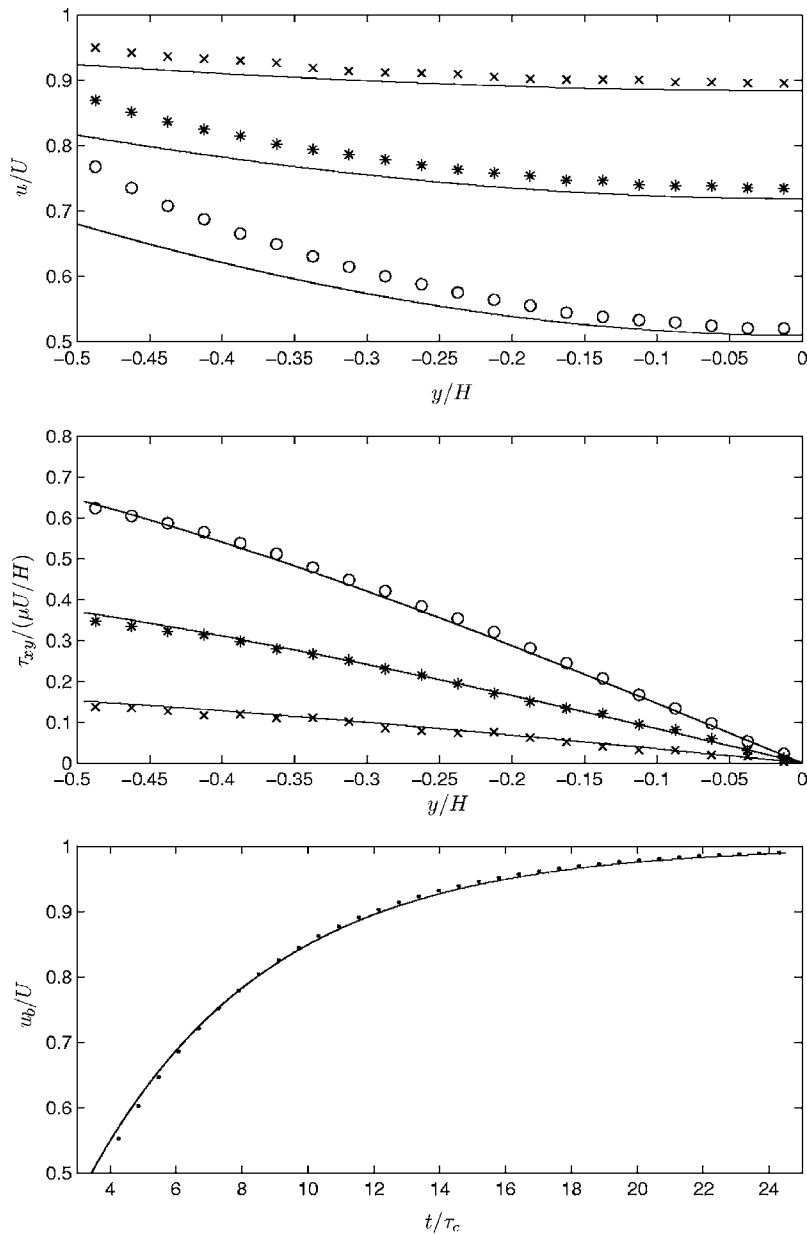


FIG. 6. Comparison between DSMC results (symbols) and second-order-slip-corrected Navier-Stokes solution (lines) for $Kn=0.35$, for the impulsive start problem described in Sec. II C 1. Due to the problem symmetry about $y=0$, only half domain is shown; the wall is at $y/H=-0.5$. Flowfield and stress plots shown at three times: $4.9\tau_c$ (\circ), $7.9\tau_c$ ($*$), and $12.8\tau_c$ (\times). Top plot: comparison of flow velocities. Middle plot: comparison of the shear stress. Bottom plot: comparison of the bulk velocity as a function of time.

Kirchhoff⁴² when the narrow channel limit is taken in the latter.

The author has recently³⁹ used the fact that wave propagation in the narrow channel limit [the narrow channel criterion needs to be suitably redefined in the transition regime where viscosity loses its meaning; however, the work in Refs. 39 and 40 shows that S remains a conservative criterion for the neglect of inertia and thermal effects for $Kn > 0.1$] is governed by the steady equation of motion to provide a prediction for the propagation constant for arbitrary Knudsen numbers without explicitly solving the Boltzmann equation. This is achieved by rewriting Eq. (14) in the form

$$\tilde{u}_b = -\frac{1}{\mathcal{R}} \frac{d\tilde{P}}{dx}, \tag{22}$$

where tilde denotes the amplitude of a sinusoidally time-varying quantity and $\mathcal{R}=\mathcal{R}(Kn)$, the “flow resistance,” is given by

$$\mathcal{R} = \frac{P_0}{H\bar{Q}\sqrt{RT_0/2}}. \tag{23}$$

Here, P_0 and T_0 denote the mean pressure and temperature, respectively. Equation (22) locally describes wave propagation since, as we argued above, in the narrow channel limit the flow is isothermal and quasistatic and governed by the steady-flow equation of motion. Using the long-wavelength approximation allows us to integrate mass conservation, written here as a kinematic condition,³⁹

$$\frac{\partial P}{\partial x} = -\left(\frac{\partial P}{\partial \rho}\right)_T \rho_0 \frac{\partial^2 \xi}{\partial x^2} \tag{24}$$

across the channel height. Here $(\partial P/\partial \rho)_T$ indicates that this derivative is evaluated under isothermal conditions appropriate to a narrow channel. Additionally, ρ_0 is the average density and ξ is the fluid-particle displacement defined by

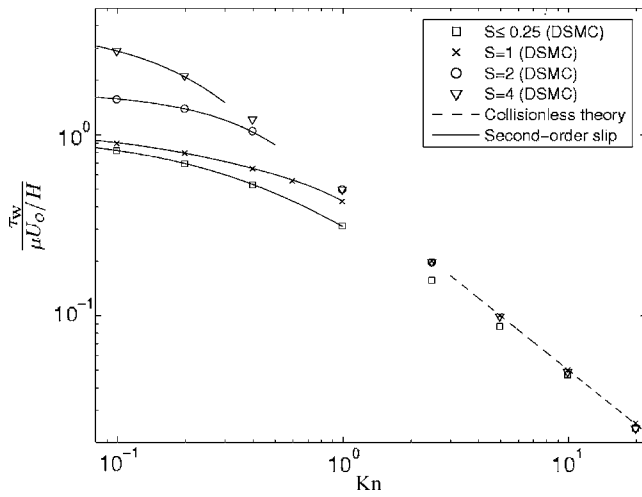


FIG. 7. Normalized wall shear stress magnitude as a function of the Knudsen number. Symbols denote DSMC results. Solid lines denote the second-order slip model result. Dashed line denotes the collisionless result. Here, the left wall oscillates with velocity amplitude U_o .

$$u_x(x, y, t) = \frac{\partial \xi(x, y, t)}{\partial t}. \quad (25)$$

Combining Eqs. (22) and (24) we obtain³⁹

$$i\omega \xi_b = \frac{\rho_0 (\partial P / \partial \rho)_T \partial^2 \xi_b}{\mathcal{R}}, \quad (26)$$

where ξ_b is the bulk (average over the channel width) fluid-particle displacement. From the above we can obtain the propagation constant

$$(m_m + ik)^2 = \frac{i\omega \mathcal{R}}{P_0}, \quad (27)$$

where m_m is the attenuation coefficient and k is the wave-number. Using Eq. (23) we obtain

$$(m_m + ik)^2 \lambda^2 = \frac{8i\sqrt{\pi} Kn \tau_c}{\bar{Q}} \frac{\tau_c}{T}, \quad (28)$$

where $T = 2\pi/\omega$ is the oscillation period.

This result is expected to be of general use because the narrow channel requirement is easily satisfied in the transition regime.³⁹ A more convenient expression for use in the early transition regime, which does not require a lookup table (for \bar{Q}), can be obtained using the second-order slip model discussed in Sec. II C 1. Using this model we obtain

$$(m_m + ik)^2 \lambda^2 = \frac{96iKn^2}{1 + 6\alpha Kn + 12\varepsilon Kn^2} \frac{\tau_c}{T}, \quad (29)$$

which, as can be seen in Fig. 8, remains reasonably accurate up to $Kn \approx 1$ (aided by the square-root dependence of the propagation constant on \mathcal{R}). This expression for $Kn \rightarrow 0$ reduces to the well-known narrow-channel result obtained using the no-slip Navier-Stokes description.⁴³

Figure 8 shows a comparison between Eq. (29) [Eq. (28)], DSMC simulations, and the Navier-Stokes result. (DSMC simulations of wave propagation are discussed in

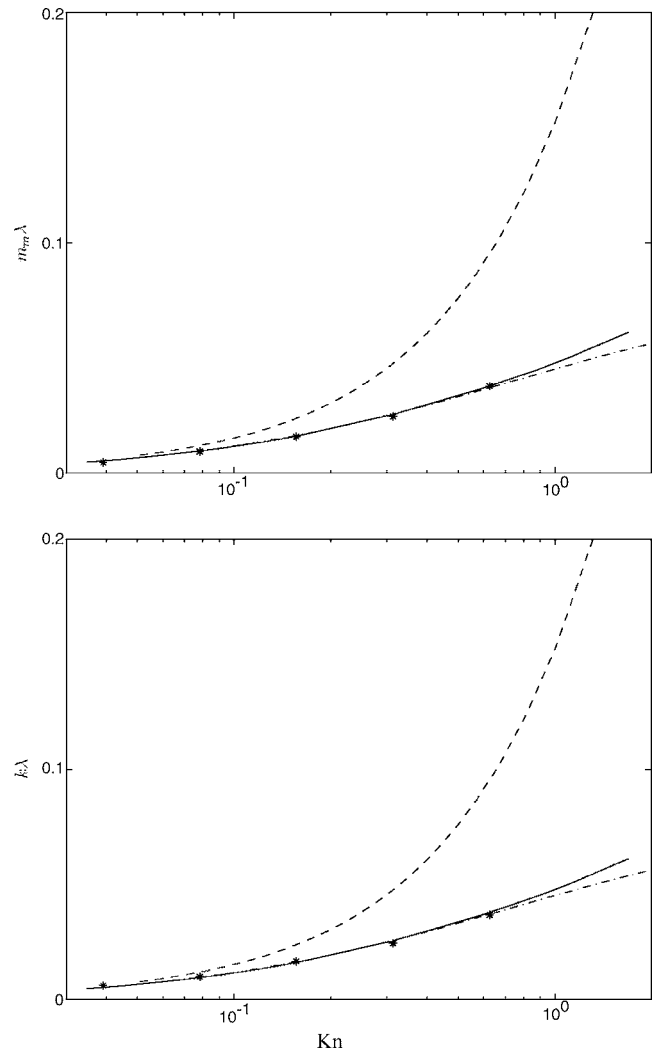


FIG. 8. Comparison between the theoretical predictions of Eq. (28), shown as a solid line, and the simulation results denoted by stars as a function of the Knudsen number at a constant frequency given by $T/\tau_c \approx 6400$. The dash-dotted line denotes the prediction of Eq. (29). The no-slip Navier-Stokes solution (dashed lines) is also included for comparison.

Ref. 39.) It can be seen that the theory is in excellent agreement with DSMC results. As noted above, the second-order slip model provides an excellent approximation for $Kn \lesssim 0.5$ and a reasonable approximation up to $Kn \approx 1$. The no-slip Navier-Stokes result clearly fails as the Knudsen number increases. The theory presented here can be easily generalized to ducts of arbitrary cross-sectional shape, and has been extended⁴⁰ to include the effects of inertia and heat transfer in the slip-flow regime where closures for the shear stress tensor and heat flux vector exist.

F. Reynolds equation for thin films

The approach of Sec. II E is reminiscent of lubrication theory analyses used in describing the flow in thin films.⁴⁴ This type of approach, typically using the Reynolds equation, is fairly common in small-scale devices whose geometry lends itself naturally to this type of analysis. An extensive discussion of the Reynolds equation and its applications to small-scale flows can be found in Ref. 37. Our objective

here is to briefly discuss the opportunities provided by the lubrication approximation for obtaining solutions for arbitrary Knudsen numbers to various small-scale problems, without explicitly solving the Boltzmann equation.

In a one-dimensional gap (see Fig. 1) with one plate moving in the x direction with velocity U_x , the Reynolds equation reads

$$\frac{\partial}{\partial x} \left[-\frac{\rho H^3}{12\mu} \frac{dP}{dx} + \frac{\rho H U_x}{2} \right] = -\frac{\partial(\rho H)}{\partial t}. \quad (30)$$

This formulation is convenient because it requires only knowledge of the flow rate (average flow speed) through the gap; this has the fortunate consequence that it can be easily generalized to arbitrary Knudsen numbers in a fashion that is exactly analogous to the procedure used in Sec. II E. This was realized by Fukui and Kaneko,⁴⁵ who formulated such a generalized Reynolds equation by:

- Realizing that the “Couette” flow contribution to the mass flow rate ($\rho H U_x/2$) does not change with the Knudsen number.
- Replacing the Navier-Stokes (Poiseuille) mass flow rate

$$-\frac{\rho H^3}{12\mu} \frac{dP}{dx}$$

by the form

$$-\frac{\rho H^2}{P} \sqrt{\frac{RT}{2}} \bar{Q}(\sigma, \text{Kn}) \frac{dP}{dx}$$

valid for all Knudsen numbers and accommodation coefficients.

- Including the flow rate due to thermal creep

$$\frac{\rho H^2}{T} \sqrt{\frac{RT}{2}} \bar{Q}_T(\sigma, \text{Kn}) \frac{dT_w}{dx}$$

(Ref. 45) into the total flow rate, and thus accounting for the effects of an axial temperature gradient.

Comparison between the formulation of Fukui and Kaneko and DSMC simulations can be found in Ref. 46.

A number of approaches using fits of $\bar{Q}(\text{Kn})$ to define an “effective viscosity” for integrating the resulting “generalized” Reynolds equation have appeared. It is hoped that the discussion of Sec. II C 1 illustrates that the concept of an “effective viscosity” is not very robust for a number of reasons (this discussion is not limited to the context of Reynolds equation applications). For $\text{Kn} \gg 0.1$ the physical mechanism of transport changes and there is no reason to expect the concept of linear-gradient transport to hold. Even in the early transition regime, the concept of an “effective viscosity” is contradicted by a variety of findings (see Sec. II C 1). To be more specific, an “effective viscosity” can be viewed as the particular choice of absorbing the kinetic corrections to the Poiseuille flow rate in Eq. (20), namely $1 + 6\alpha\text{Kn} + 12\varepsilon\text{Kn}^2$, into one of the proportionality constants, namely the viscosity. However, Sec. II C 1 has shown that the origin of these corrections (first- and second-order slip and Knudsen layer contribution to the flow rate) is not consistent with a variable

viscosity. In fact, the correct way of interpreting Eq. (20) is that the constitutive relation, including the value of the viscosity, remain unchanged up to at least $\text{Kn} \approx 0.4$. Moreover, when the “effective viscosity” approach is adopted, the following problems arise:

- Kinetic corrections to the flow rate are problem dependent (flow, geometry); as a result, an effective viscosity approach cannot be predictive. For example, the “effective viscosity” fitted from the Poiseuille flow rate in a tube is different from the “effective viscosity” fitted from the Poiseuille flow rate in a channel due to the curvature corrections to the second-order slip coefficient discussed in Sec. II C 1.
- The fitted “effective viscosity” does not give the correct stress through the linear constitutive law.

The “effective viscosity” approach has another disadvantage when used in the Reynolds equation: the complex expressions used to fit \bar{Q} typically cannot be directly integrated, unless the assumption $\text{Kn} \neq \text{Kn}(P)$ is made. Use of Eq. (21) for $\text{Kn} \leq 0.5$, on the other hand, should not suffer from this disadvantage.

G. Flows involving heat transfer

In this section we review flows in which heat transfer is important. We give particular emphasis to *convective* heat transfer in internal flows, which has only recently been investigated within the context of Navier-Stokes failure in small-scale gaseous flows. We also summarize the investigation of Gallis and co-workers on thermophoretic forces on small particles in gas flows.

1. The Graetz problem for arbitrary Knudsen numbers

Since its original solution in 1885 (Ref. 47), the Graetz problem has served as an archetypal convective heat-transfer problem both from a process modeling and an educational viewpoint. In the Graetz problem a fluid is flowing in a long channel whose wall temperature changes in a step fashion. The channel is assumed to be sufficiently long so that the fluid is in an isothermal and hydrodynamically fully developed state before the wall temperature changes. One is typically interested in the energy exchange between the walls and the gas, which can be quantified by the Nusselt number

$$\text{Nu}_T = \frac{q2H}{\kappa(T_w - T_b)}, \quad (31)$$

which is a nondimensional heat-transfer coefficient.⁴⁸ Here q is the wall heat flux and T_b is the bulk temperature defined by

$$T_b = \frac{\int_{-H/2}^{H/2} u_x T dy}{u_b H}. \quad (32)$$

Although the work in Ref. 50 focused on the fully developed Nusselt number, the developing (tube entrance) part of the flow can also be treated using the same approach.

The gas-phase Graetz problem subject to slip-flow boundary conditions was studied originally by Sparrow;⁴⁹ this study, however, did not include the effects of axial heat

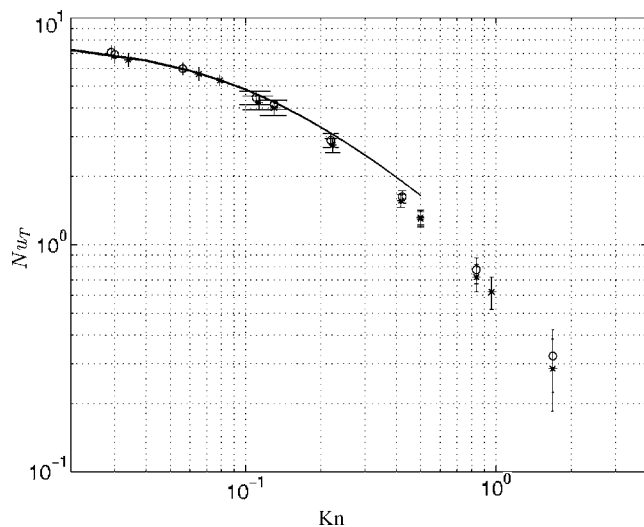


FIG. 9. Variation of Nusselt number Nu_T with Knudsen number Kn (from Ref. 50). The stars denote DSMC simulation data for increasing wall temperature and the circles denote DSMC simulation data for decreasing wall temperature. The (overlying) solid lines denote hard-sphere slip-flow results for $Pe=0.01, 0.1, \text{ and } 1.0$.

conduction which cannot be neglected in small-scale flows. Here we review the solution by the author,⁵⁰ in which the extended Graetz problem [including the effect of axial heat conduction parametrized by the Peclet number $Pe = RePr = (\rho u_b 2H / \mu) Pr$] is solved in the slip-flow regime. The solution is compared to DSMC simulations in a wide range of Knudsen numbers; the DSMC solutions serve to verify the slip-flow solution but also extend the Graetz solution to the transition regime. The DSMC simulations were performed at sufficiently low speeds for the effects of viscous heat dissipation to be small; this is very important since high speeds typically used in DSMC simulations to alleviate signal-to-noise limitations (a new method for solving the Boltzmann equation, which does not suffer from this limitation, is discussed in Sec. III E) may introduce sufficient viscous heat dissipation effects to render the simulation results invalid. The effect of viscous dissipation on convective heat transfer is briefly discussed at the end of this section.

In Ref. 50 a semianalytical solution of the Graetz problem in the slip-flow regime for all Peclet numbers was presented. This solution showed that in the presence of axial heat conduction ($Pe \leq 10$) the Nusselt number is larger than the corresponding Nusselt number in the absence of axial heat conduction ($Pe \rightarrow \infty$). In particular, it was found that for typical small-scale applications where $Pe < 1$ the Nusselt number is fairly insensitive to the Peclet number, but higher (by about 10%) than $Nu(Pe \rightarrow \infty)$.

The semianalytical slip-flow solution of Ref. 50 was complemented by low-speed DSMC simulations in both the slip-flow and transition regimes (see Fig. 9). Comparison of the two solutions in the slip-flow regime shows that the effects of thermal creep are negligible for typical conditions, and also that the velocity slip and temperature jump coefficients of Sec. II A provide good accuracy in this regime. The DSMC solutions in the transition regime showed that for fully accommodating walls the Nusselt number decreases

monotonically with increasing Knudsen number. Unpublished DSMC solutions for accommodation coefficients smaller than one exhibit the same qualitative behavior as partially accommodating slip-flow results; in other words, decreasing the thermal accommodation coefficient increases the thermal resistance and decreases the Nusselt number, while decreasing the momentum accommodation coefficient increases the flow velocity close to the wall leading to a small increase in the Nusselt number.⁵⁰ The similarity between the Nusselt number dependence on the Knudsen number and the dependence of the skin-friction coefficient on the Knudsen number⁵⁰ suggests that some form of Reynolds analogy between the two nondimensional numbers may exist for $Kn \geq 0.1$.

The effect of viscous dissipation on convective heat transfer is typically quantified by the Brinkman number $Br = \mu u_b^2 / (\kappa \Delta T)$, where ΔT is the characteristic temperature difference in the flow. It is well known that viscous dissipation in the fluid affects convective heat transfer both in terms of bulk temperature fields and resulting Nusselt numbers. Dissipation in small-scale flows is interesting both from practical and theoretical points of view. It becomes especially relevant in view of the limitations associated with DSMC, which require artificially high flow velocities in order to obtain a discernible hydrodynamic signal. From a theoretical point of view, small-scale (slipping) flows differ from their large-scale (nonslipping) counterparts because the slip present at the system boundaries leads to an additional mode of dissipation, namely, shear work at the boundary. In Ref. 51 the author presented an analysis of a model convective heat-transfer problem, namely convective heat transfer under constant wall heat flux⁴⁸—a dual to the Graetz problem described above—in the presence of dissipation: it was shown that, in the slip-flow regime, shear work on the boundary scales with the Brinkman number Br , similarly to viscous heat dissipation in the bulk; also, although shear work at the boundary must be included in the total heat exchange with the system walls, it has no direct influence on the bulk temperature field, because it occurs at the system boundaries. Consequently, it was demonstrated how shear work at the boundary can be accounted for in convective heat-transfer calculations under the assumption of (locally) fully developed conditions. It was also shown that, as the Knudsen number increases, this mode of dissipation can be as important as dissipation in the bulk of the flow.

2. Thermophoretic force on small particles

Small particles in a gas through which heat flows experience a thermophoretic force in the direction of the heat flux; this force is a result of the net momentum transferred to the particle due to the asymmetric velocity distribution of the surrounding gas⁵² in the presence of a heat flux. This phenomenon was first described by Tyndall⁵³ and has become of significant interest in connection with contamination of microfabrication processes by small solid particles. This problem appears to be particularly important in plasma-based processes which generate small particles.⁵²

Considerable progress has been made in describing this phenomenon by assuming a spherical (radius R) and infinitely conducting particle in a quiescent monoatomic gas. Provided that the particle is sufficiently small, such that it has no effect on the molecular distribution function of the surrounding gas, the thermophoretic force can be calculated by integrating the momentum flux imparted by the molecules striking the particle. The particle can be considered sufficiently small when the Knudsen number based on the particle radius, $\text{Kn}_R = \lambda/R$, implies a free-molecular flow around the particle, i.e., $\text{Kn}_R \gg 1$. Based on these assumptions, Gallis and his collaborators⁵⁴ have also developed a general method for calculating forces on particles in DSMC simulations of arbitrary gaseous flows, provided the particle concentration is dilute. This method is briefly discussed in Sec. III C.

In the cases where the molecular velocity distribution function is known, such as free-molecular flow or the Navier-Stokes limit, the thermophoretic force can be obtained analytically. Performing the calculations in these two extremes and under the assumption that the particle surface is fully accommodating, reveals that the thermophoretic force can be expressed in the following form:

$$F_{\text{th}} = \chi \pi R^2 q \bar{c}, \quad (33)$$

where χ is a thermophoresis proportionality parameter which obtains the values $\chi_{\text{FM}} = 0.75$ for free-molecular flow and $\chi_{\text{CE}} = 32/(15\pi) = 0.679$ for a Chapman-Enskog distribution for Maxwellian molecules. (Maxwellian molecules are defined such that the interaction force between them scales with the fifth power of the distance between their centers.⁴ Although not very realistic, this model was introduced by Maxwell because it makes the product $g\psi d^2\Omega$ independent of g , allowing analytical evaluation of certain functionals involving the collision integral.) Here, q is the local heat flux. Writing the thermophoretic force in the above form is, in fact, very instructive.⁵² It shows that the force is only very mildly dependent on the velocity distribution function with only a change of order 10% observed between $\text{Kn} \ll 1$ and $\text{Kn} \gg 1$. These conclusions extend to other collision models; for example, for a hard-sphere gas, $\chi_{\text{CE}} = 0.698$ (Ref. 52).

The two limiting values can be used to provide bounds for the value of the thermophoretic force on fully accommodating particles close to system walls. Using the weak dependence of χ on the distribution function, Gallis *et al.*⁵² provided an estimate of this quantity in the Knudsen layer, χ_{KN} , by assuming that the distribution function can be written as a superposition of a Chapman-Enskog (incoming and outgoing molecules) and Maxwellian distribution (outgoing molecules), with the relative proportions determined by the accommodation coefficient at the wall surface. More specifically, they consider a wall at temperature T_w with accommodation coefficient σ . For Maxwell molecules, they find

$$\chi_{\text{KN}} = \frac{1}{2} \left[\sigma \chi_{\text{CE}} + (2 - \sigma) \chi_{\text{FM}} \left(\frac{2}{1 + \sqrt{T_w/T}} \right) \right], \quad (34)$$

which simplifies to

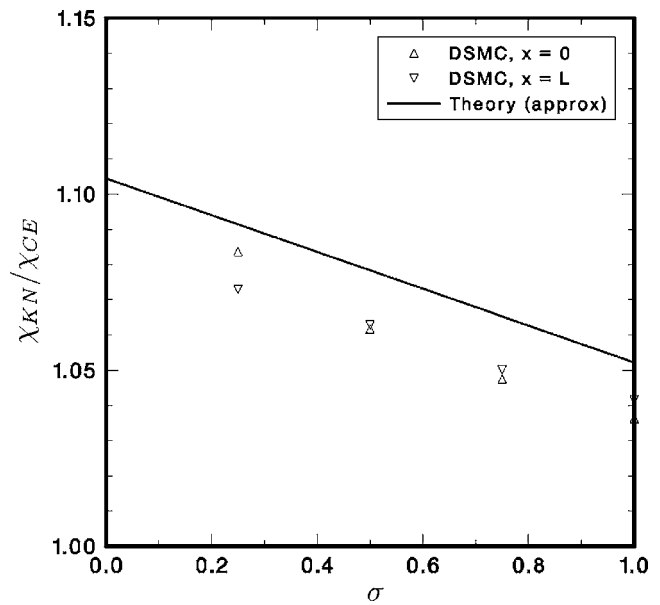


FIG. 10. Comparison between the approximate theory of Gallis and co-workers for the thermophoretic force in the Knudsen layer and DSMC results. The theoretical value for the thermophoretic force ratio (for Maxwellian molecules), $\chi_{\text{KN}}/\chi_{\text{CE}}$, is shown as a solid line. The DSMC results represent the average value over five cells of size $\Delta x = 0.042\lambda$ adjacent to the wall (there are two wall locations) in a $\text{Kn} = 0.0475$ calculation.

$$\chi_{\text{KN}} = \frac{1}{2} [\sigma \chi_{\text{CE}} + (2 - \sigma) \chi_{\text{FM}}] \quad (35)$$

in the limit $T \rightarrow T_w$, where, here T is the temperature of the gas outside the Knudsen layer. In other words, the presence of a Knudsen layer has a very small effect on the thermophoresis parameter, with $\chi_{\text{KN}} = 0.5(\chi_{\text{CE}} + \chi_{\text{FM}})$ for a fully accommodating wall and $\chi_{\text{KN}} = \chi_{\text{FM}}$ in the specular reflection limit.

DSMC simulations show⁵² that the deviation from χ_{CE} increases with proximity to the wall, as expected; they also show (see Fig. 10) that Eq. (35) serves as an upper bound to the actual thermophoresis parameter within the Knudsen layer; this is presumably because the assumed distribution function overestimates the deviation from the actual distribution.

III. NUMERICAL METHODS

In this section we briefly discuss recent developments in the numerical solution of the Boltzmann equation. The majority of these developments is associated with the direct simulation Monte Carlo, briefly discussed below, since this is by far the most popular approach for dilute gases. In the interests of brevity we will not discuss hybrid Boltzmann-Navier-Stokes methods, which increase computational efficiency by limiting the use of the Boltzmann treatment to the regions where it is needed; discussions of hybrid methods can be found in Refs. 55 and 56. We will close this section with a description of a new variance reduction technique developed to address the computational intransigence of DSMC in low-speed flows resulting from the slow convergence rate associated with statistical sampling of macroscopic properties.

A. The direct simulation Monte Carlo

The direct simulation Monte Carlo is a stochastic particle simulation technique⁹ for solving the nonlinear Boltzmann equation.⁵⁷ DSMC solves the Boltzmann equation by applying a splitting approach to the motion of the particle simulators (each particle simulates a large number of real molecules) comprising the system; the time evolution of the system is approximated by a sequence of discrete time steps of duration Δt , in which particles successively undergo collisionless advection and collisions. Collisions take place between collision partners selected randomly within cells of size Δx . The introduction of the above approach with the associated discretization ingredients ($\Delta t, \Delta x$) eliminates the computational cost associated with calculating exact particle trajectories and leads to a simulation method that is significantly more efficient than “brute force” molecular dynamics approaches.

An augmented DSMC formulation which extends the applicability of DSMC to gases of moderate densities, where molecular size effects are not negligible, has also been developed⁵⁸ and is known as the “consistent Boltzmann algorithm.”

B. The effect of finite discretization in DSMC

DSMC has been used to capture and predict nonequilibrium hydrodynamic phenomena in all Knudsen regimes⁹ for more than three decades. However, it is only recently that significant progress has been made in its characterization as a numerical method and in understanding the numerical errors associated with it.

Recently, Wagner⁵⁷ has shown that DSMC simulations approach solutions of the nonlinear Boltzmann equation in the limit of zero cell size and time step and infinite number of molecules. This result essentially proves “consistency.” Convergence results for the transport coefficients have been recently obtained by Alexander *et al.*⁵⁹ for the cell size, and Hadjiconstantinou⁶⁰ for the time step.

Alexander *et al.*⁵⁹ used the Green-Kubo theory to evaluate the transport coefficients in DSMC when the cell size is finite but the time step is negligible. They found that because DSMC allows collisions between molecules at a distance (as long as they are within the same cell) the transport coefficients—when measured using the heat flux at the wall⁶¹—deviate from the dilute-gas Enskog values quadratically with the cell size. For example, for the viscosity Alexander *et al.*⁵⁹ find

$$\mu = \frac{5}{16\sigma^2} \sqrt{\frac{mkT}{\pi}} \left(1 + \frac{16}{45\pi} \frac{\Delta x^2}{\lambda^2} \right). \quad (36)$$

In Ref. 60, the author considered the convergence with respect to a finite time step when the cell size is negligible. Because DSMC is discrete in time, in order to apply the Green-Kubo formulation the author developed a continuous-time analog of DSMC. Using this continuous-time analog, and the fact that the DSMC dynamics appears symmetric at the long times associated with diffusive transport coefficients, the author was able to show that the transport coeffi-

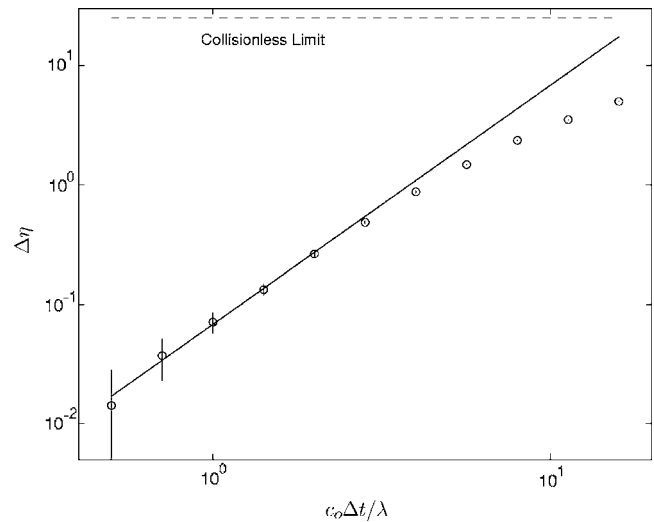


FIG. 11. Error in coefficient of viscosity as a function of normalized time step $c_o\Delta t/\lambda$ (from Ref. 62). Circles denote the normalized error in momentum flux in the simulations of Garcia and Wagner (Ref. 62), and the solid line is the prediction of (37). Note that as the time step increases, the transport rate asymptotes to the collisionless limit value.

icients deviate from the dilute-gas Enskog values proportionally to the square of the time step. For example, for the viscosity he found

$$\mu = \frac{5}{16\sigma^2} \sqrt{\frac{mkT}{\pi}} \left(1 + \frac{16}{75\pi} \frac{(c_o\Delta t)^2}{\lambda^2} \right), \quad (37)$$

where $c_o = \sqrt{2k_bT/m}$ is the most probable molecular speed. This prediction for the viscosity, and similar predictions for the thermal conductivity and diffusion coefficient derived in Ref. 60, were verified by DSMC simulations.⁶² Good agreement was found between theory and simulation as illustrated in the example of Fig. 11. The theoretical result for the thermal conductivity was also recently verified by Rader *et al.*;⁶¹ by studying a number of variants of the DSMC algorithm, these authors also verify that the above results are observed when sampling is performed in a fashion which is consistent with the symmetry in the dynamics.

The study by Rader *et al.*⁶¹ also reports a discretization error due to a finite number of particles in a cell. The best fit to their numerical result for the deviation from the theoretical value of the thermal conductivity, in the limit $\Delta x, \Delta t \rightarrow 0$, gives the leading-order term to be $-0.083/N$.

C. Forces on small spherical particles in DSMC

One of the most important challenges associated with semiconductor manufacturing is the presence of contaminants, sometimes produced during the manufacturing process, in the form of small particles. Understanding the transport of these particles is very important for their removal or their handling in ways which ensure that they do not interfere with the manufacturing process. Recently, Gallis and his co-workers⁵⁴ developed a method for calculating the force on small particles in rarefied flows simulated by DSMC. This method is based on the assumption that the particle concentration is very small and the observation that particles with

sufficiently small radius such that $\text{Kn}_R = \lambda/R \gg 1$ will have a very small effect on the flowfield; in this case, the effect of the flowfield on the particles can be calculated from DSMC simulations which do not include the particles themselves.

Gallis and his co-workers define appropriate ‘‘Green’s functions’’ which quantify the momentum $\mathbf{F}_g[\tilde{\mathbf{c}}]$ and energy $Q_g[\tilde{\mathbf{c}}]$ transfer rates of individual molecules to the particle surface as a function of the molecule mass, momentum and energy, and degree of accommodation on the particle surface. These can then be integrated over the molecular velocity distribution function, $f(\tilde{\mathbf{c}})$, to yield the average force

$$\mathbf{F} = \int \mathbf{F}_g[\tilde{\mathbf{c}}]f(\tilde{\mathbf{c}})d\tilde{\mathbf{c}} \quad (38)$$

or heat flux

$$q = \int Q_g[\tilde{\mathbf{c}}]f(\tilde{\mathbf{c}})d\tilde{\mathbf{c}} \quad (39)$$

to the particle, where $\tilde{\mathbf{c}} = \mathbf{c} - \mathbf{u}_p$ and \mathbf{u}_p is the particle speed.

For the case of Maxwell’s gas-surface interaction, Gallis *et al.*⁵⁴ find

$$\mathbf{F}_g[\tilde{\mathbf{c}}] = \rho\pi R^2 \tilde{\mathbf{c}}(|\tilde{\mathbf{c}}| + \sigma(\pi^{1/2}/3)c_o^p), \quad (40)$$

$$Q_g[\tilde{\mathbf{c}}] = \sigma\rho\pi R^2 |\tilde{\mathbf{c}}|((1/2)|\tilde{\mathbf{c}}|^2 - (c_o^p)^2), \quad (41)$$

where $c_o^p = \sqrt{2k_b T_p/m}$ and T_p is the particle temperature. More complex accommodation models can also be treated; in Ref. 54 an extended Maxwell accommodation model is presented.

In the DSMC implementation, integration of Eqs. (38) and (39) is achieved by summing the contributions of molecules within a cell. This yields the force and heat flux to a particle as a function of position. Because the force and heat flux are a function of \mathbf{u}_p , the former are calculated as a function of a number of values of the latter; the values of the force and heat flux at intermediate values of \mathbf{u}_p can be subsequently obtained by interpolation.⁵⁴

D. Statistical noise in low-speed flows

In a recent paper, Hadjiconstantinou *et al.*⁶³ used equilibrium statistical mechanics to obtain theoretical results for the relative statistical (sampling) error in hydrodynamic quantities in molecular simulations of flows close to equilibrium. These results characterize the dependence of the relative statistical error $E_Q = \sigma_Q/\langle Q \rangle$ of hydrodynamic quantity Q on gas properties and the number of samples taken; here $\langle Q \rangle$ is the mean value of Q and σ_Q is the standard deviation in the error in estimating $\langle Q \rangle$. Such results are useful because DSMC, the prevalent solution method for the Boltzmann equation, relies on statistical sampling for extracting hydrodynamic fields from particle data. In fact, perhaps the biggest disadvantage associated with DSMC stems from the large relative statistical error present in low-speed flows where the deviation from equilibrium is small. A variance reduction method developed to reduce statistical uncertainty is described in the next section.

In Ref. 63 a variety of expressions for the relative statistical error for the most common hydrodynamic state variables and their fluxes (shear stress, heat flux) was derived. For example, it was shown that the statistical uncertainty in the flow velocity is given by

$$E_u = \frac{\sigma_u}{\langle u \rangle} = \frac{1}{\sqrt{\gamma \text{Ma} \sqrt{NM}}}, \quad (42)$$

where N is the number of particles in the sampling volume and M is the number of independent samples per particle. For the hydrodynamic fluxes, expressions were derived when those are measured as volume averages and when measured as surface flux averages. The main findings of this work can be summarized as follows:

- (1) The two averaging methods for hydrodynamic fluxes (volume, surface) yield comparable relative statistical errors, provided that $\Delta x \approx c_o \Delta t$. Here Δt is the averaging time used in the flux method; Δx is the linear dimension, in the direction normal to the flux, of the cell in which volume averaging is performed.
- (2) For $\text{Kn} \ll 1$, the relative error in a particular hydrodynamic flux (e.g., shear stress) is significantly larger than the relative error in the ‘‘conjugate’’ state variable (e.g., velocity).
- (3) A simple theory for incorporating the effects of correlations in volume averaging was presented. This theory is based on the theory of persistent random walks.
- (4) It was shown that not only the number of molecules per unit volume in an ideal gas is Poisson distributed, but also arbitrary number fluctuations of an infinite ideal gas in equilibrium are Poisson distributed.

Good agreement was found with DSMC simulations of low-speed, low Knudsen number flows where statistical noise presents the biggest challenges. This is expected since the deviation from equilibrium is small under these conditions. The results for state variables were also verified for dense fluids using molecular dynamics simulations.

E. Variance reduction

Equation (42) shows that for a given statistical uncertainty, the computational cost in DSMC scales as Ma^{-2} . As a result, the simulation of low-speed flows at negligible statistical uncertainty is prohibitively expensive unless massively parallel computer resources are available: for example, to obtain 1% statistical uncertainty in a 1 m/s flow at typical temperatures, one would need on the order of 5×10^8 independent samples per cell.⁶³

To address the inefficiency of DSMC for low-speed flows, Baker and Hadjiconstantinou developed a variance reduction technique for calculating the collision integral of the Boltzmann equation which exploits the fact that, in these flows, the deviation from equilibrium is small. More specifically, they showed that one can construct methods that are significantly more efficient by focusing the computational effort on calculating the value of the collision integral due to the deviation from equilibrium, since the value of the colli-

sion integral at equilibrium is zero. This can be achieved by evaluating the following “variance-reduced” form of the collision integral:

$$\left[\frac{df}{dt} \right]_{\text{coll}} = \frac{1}{2} \int \int \int (\delta'_1 + \delta'_2 - \delta_1 - \delta_2) \times (2f_1^{\text{MB}} + f_1^d) f_2^d \psi d^2 \Omega d^3 \mathbf{v}_1 d^3 \mathbf{v}_2, \quad (43)$$

where $f^d = f - f^{\text{MB}}$ is the deviation from any chosen equilibrium (Maxwell-Boltzmann) distribution f^{MB} .

The above expression is obtained⁶⁴ by expanding f about this equilibrium state in the following form⁷ of the collision integral:

$$\left[\frac{df}{dt} \right]_{\text{coll}} = \frac{1}{2} \int \int \int (\delta'_1 + \delta'_2 - \delta_1 - \delta_2) \times f_1 f_2 g \psi d^2 \Omega d^3 \mathbf{v}_1 d^3 \mathbf{v}_2 \quad (44)$$

and noticing that the value of the collision integral for any equilibrium distribution is identically zero, i.e.,

$$\frac{1}{2} \int \int \int (\delta'_1 + \delta'_2 - \delta_1 - \delta_2) f_1^{\text{MB}} f_2^{\text{MB}} g \psi d^2 \Omega d^3 \mathbf{v}_1 d^3 \mathbf{v}_2 = 0. \quad (45)$$

Here, $f_1 \equiv f(\mathbf{x}, \mathbf{v}_1, t)$, $f_2 \equiv f(\mathbf{x}, \mathbf{v}_2, t)$, $\delta_1 \equiv \delta(\mathbf{v} - \mathbf{v}_1)$, $\delta_2 \equiv \delta(\mathbf{v} - \mathbf{v}_2)$, $\delta'_1 \equiv \delta(\mathbf{v} - \mathbf{v}'_1)$, $\delta'_2 \equiv \delta(\mathbf{v} - \mathbf{v}'_2)$, where a prime indicates postcollision velocities and δ is the Dirac delta function.

When the deviation from equilibrium is small, the variance reduction achieved by evaluating (43) by a Monte Carlo method instead of (44) is large. Moreover, the degree of variance reduction is larger for distributions that are closer to the equilibrium distribution, leading to a method that can practically capture very small deviations from equilibrium. This is in sharp contrast to methods that do not use f^d in evaluating the collision integral (such as DSMC). In DSMC in particular, as $f^d \rightarrow 0$, f^{MB} dominates the integrand landscape and thus leads to a constant statistical noise,⁶³ which in turn means that the signal-to-noise ratio decreases linearly⁶³ with decreasing Mach number [see Eq. (42)]. On the other hand, in the method presented here, the integrand landscape and consequently the statistical error⁶⁵ scale with f^d in the limit $f^d \rightarrow 0$; as a result, in this limit, the statistical error decreases linearly with the signal leading to a constant signal-to-noise ratio.⁶⁴ This is shown in Fig. 12, which compares the relative statistical uncertainty of the present method with that of DSMC as a function of the characteristic flow velocity for a shear flow.

It was shown in Ref. 64 that the Boltzmann equation can be numerically solved using this approach for evaluating the collision integral and by discretizing the advection operator using a finite volume or finite difference method. In Ref. 66 the same authors show how variance reduction ideas can be used to derive a DSMC-like (particle) scheme for solving the Boltzmann equation, namely by simulating particles which represent *deviation from equilibrium*.

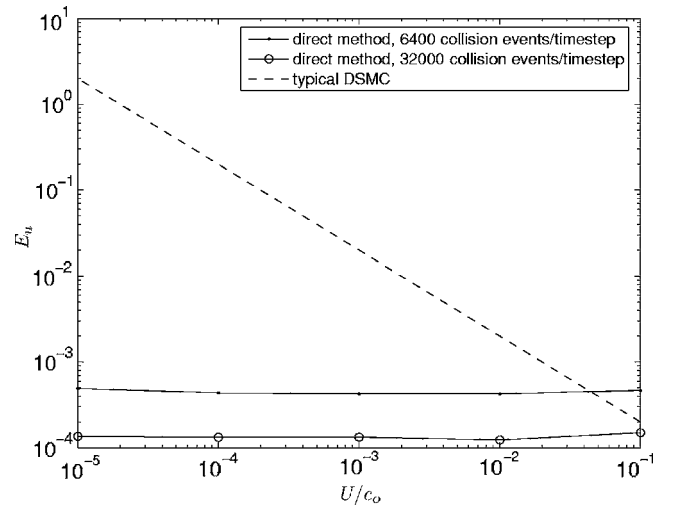


FIG. 12. Relative statistical uncertainty in flow velocity (averaged over the flow domain) as a function of the wall velocity, U , in Couette flow. Note that the number of samples required to make the statistical uncertainty of the two methods the same, scales with the *square* of the ratio of statistical uncertainties.

IV. DISCUSSION

Theoretical solutions of various phenomena involving isothermal and nonisothermal flows suggest that slip flow is remarkably robust. In channel flows, slip flow seems to correctly predict *average* quantities of interest (flow rates, wave propagation constants, heat-transfer coefficients) even beyond its typically acknowledged limit of applicability of $\text{Kn} \approx 0.1$ with acceptable error; moreover, in some cases it can *qualitatively* describe the behavior of such *average* quantities well into the transition regime.

Methods that extend the range of applicability of the Navier-Stokes description even beyond first-order slip flow are highly desirable. The simplicity and significant computational efficiency advantage enjoyed by the Navier-Stokes description compared to molecular approaches, coupled with the effort already invested in continuum methods, make the former the approach of choice. Despite the lack of general closure models for transport in the transition regime, analytical solutions are sometimes possible through the use of the lubrication approximation and judicious use of already existing analytical results for simple flows. Rigorous high-order slip models such as the one presented in Sec. II C 1 are proving to be valuable in this respect.

Direct simulation Monte Carlo has played and will continue to play a central role in the analysis of small-scale, internal gaseous flows. The statistical sampling employed by this method and the slow convergence associated with it, is, perhaps, the most serious limitation of DSMC in the context of small-scale, low-speed flows. Variance reduction techniques such as the one described in Sec. III E have the potential to completely eliminate this limitation.

Significant effort should be invested in carefully evaluating commonly used gas-surface interaction models such as Maxwell’s model; although more sophisticated gas-surface interaction models have been developed,¹⁵ and have been shown to be sufficiently tractable for numerical

implementation,^{67,68} experimental verification of their ability to produce accurate results that are also superior to the ones obtained using the simple Maxwell model, is lacking. More realistic models should be developed if these are found to be insufficient.

ACKNOWLEDGMENTS

The author wishes to thank T. R. Akylas, A. Beskok, A. L. Garcia, J. Lienhard V, and A. T. Patera for helpful comments and discussions. Special thanks to M. A. Gallis for critically commenting on the manuscript. This work was supported in part by the Center for Computational Engineering, and the Center for Advanced Scientific Computing, Lawrence Livermore National Laboratory, U.S. Department of Energy, Contract No. W-7405-ENG-48, and by Sandia National Laboratory.

- ¹C. M. Ho and Y. C. Tai, "Micro-electro-mechanical systems (MEMS) and fluid flows," *Annu. Rev. Fluid Mech.* **30**, 579 (1998).
- ²G. E. Karniadakis and A. Beskok, *Microflows: Fundamentals and Simulation* (Springer, New York, 2001).
- ³M. Gad-el-Hak, "Flow physics," in *Handbook of MEMS*, edited by M. Gad-el-Hak (CRC, Boca Raton, FL, 2002).
- ⁴W. G. Vincenti and C. H. Kruger, *Introduction to Physical Gas Dynamics* (Krieger, Malabar, FL, 1965).
- ⁵S. Chapman and T. G. Cowling, *The Mathematical Theory of Non-Uniform Gases* (Cambridge University Press, Cambridge, England, 1970).
- ⁶Y. Sone, *Kinetic Theory and Fluid Dynamics* (Birkhäuser, Boston, 2002).
- ⁷C. Cercignani, *The Boltzmann Equation and Its Applications* (Springer-Verlag, New York, 1988).
- ⁸H. Grad, "Singular and nonuniform limits of solutions of the Boltzmann equation," in *Transport Theory, Proceedings of the 20th Symposium in Applied Mathematics, New York, NY, 1967*, SIAM-AMS Proceedings Vol. 1, edited by R. Bellman, G. Birkhoff, and I. Abu-Shumays (American Mathematical Society, Providence, 1969).
- ⁹G. A. Bird, *Molecular Gas Dynamics and the Direct Simulation of Gas Flows* (Clarendon, Oxford, 1994).
- ¹⁰P. L. Bhatnagar, E. P. Gross, and M. Krook, "A model for collision processes in gases," *Phys. Rev.* **94**, 511 (1954).
- ¹¹F. J. Alexander and A. L. Garcia, "The direct simulation Monte Carlo method," *Comput. Phys.* **11**, 588 (1997).
- ¹²M. N. Kogan, *Rarefied Gas Dynamics* (Plenum, New York, 1969).
- ¹³E. Kennard, *Kinetic Theory of Gases* (McGraw-Hill, New York, 1938).
- ¹⁴F. Sharipov and V. Seleznev, "Data on internal rarefied gas flows," *J. Phys. Chem. Ref. Data* **27**, 657 (1998).
- ¹⁵C. Cercignani and M. Lampis, "Kinetic models for gas-surface interactions," *Transp. Theory Stat. Phys.* **1**, 101 (1971).
- ¹⁶C. Cercignani, P. Foresti, and F. Sernagiotto, "Dependence of the slip coefficient on the form of the collision frequency," *Nuovo Cimento B* **57**, 297 (1968).
- ¹⁷T. E. Wenski, T. Olson, C. T. Rettner, and A. L. Garcia, "Simulations of air slider bearings with realistic gas-surface scattering," *J. Tribol.* **120**, 639 (1998).
- ¹⁸T. Ohwada, Y. Sone, and K. Aoki, "Numerical analysis of the Poiseuille and thermal transpiration flows between parallel plates on the basis of the Boltzmann equation for hard-sphere molecules," *Phys. Fluids A* **1**, 2042 (1989).
- ¹⁹C. Cercignani, "The Kramers problem for a not completely diffusing wall," *J. Math. Anal. Appl.* **10**, 568 (1965).
- ²⁰S. K. Loyalka, "Momentum and temperature-slip coefficients with arbitrary accommodation at the surface," *J. Chem. Phys.* **48**, 5432 (1968).
- ²¹Y. Sone, "Kinetic theory analysis of linearized Rayleigh problem," *J. Phys. Soc. Jpn.* **19**, 1463 (1964).
- ²²C. Cercignani, "Higher order slip according to the linearized Boltzmann equation," Institute of Engineering Research Report No. AS-64-19, University of California, Berkeley, 1964.
- ²³E. B. Arkilic, K. S. Breuer, and M. A. Schmidt, "Mass flow and tangential momentum accommodation in silicon micromachined channels," *J. Fluid Mech.* **437**, 29 (2001).
- ²⁴C. Aubert and S. Colin, "High-order boundary conditions for gaseous flows in rectangular microducts," *Microscale Thermophys. Eng.* **5**, 41 (2001).
- ²⁵J. Maurer, P. Tabeling, P. Joseph, and H. Willaime, "Second-order slip laws in microchannels for helium and nitrogen," *Phys. Fluids* **15**, 2613 (2003).
- ²⁶M. Knudsen, "Die Gesetze der molecular Stromung und die inneren Reibungstromung der Gase durch Rohren," *Ann. Phys.* **28**, 75 (1909).
- ²⁷C. Cercignani and A. Daneri, "Flow of a rarefied gas between two parallel plates," *J. Appl. Phys.* **34**, 3509 (1963).
- ²⁸A. Beskok and G. E. Karniadakis, "A model for flows in channels and ducts at micro and nano scales," *Microscale Thermophys. Eng.* **3**, 43 (1999).
- ²⁹R. G. Deissler, "An analysis of second-order slip flow and temperature-jump boundary conditions for rarefied gases," *Int. J. Heat Mass Transfer* **7**, 681 (1964).
- ³⁰A. Srekanth, "Slip flow through long circular tubes," in *Proceedings of the Sixth International Symposium on Rarefied Gas Dynamics*, edited by L. Trilling and H. Y. Wachman (Academic, New York, 1969), Vol. 1, pp. 667-680.
- ³¹Y. Sone, "Asymptotic theory of flow of rarefied gas over a smooth boundary I," in *Proceedings of the Sixth International Symposium on Rarefied Gas Dynamics* (Academic, New York, 1969), Vol. 1, pp. 243-253.
- ³²N. G. Hadjiconstantinou, "Comment on Cercignani's second order slip coefficient," *Phys. Fluids* **15**, 2352 (2003).
- ³³T. Ohwada, Y. Sone, and K. Aoki, "Numerical analysis of the shear and thermal creep flows of a rarefied gas over a plane wall on the basis of the linearized Boltzmann equation for hard-sphere molecules," *Phys. Fluids A* **1**, 1588 (1989); Y. Sone, T. Ohwada, and K. Aoki, "Temperature jump and Knudsen layer in a rarefied gas over a plane wall: Numerical analysis of the linearized Boltzmann equation for hard-sphere molecules," *ibid.* **1**, 363 (1989).
- ³⁴N. G. Hadjiconstantinou, "Validation of a second-order slip model for dilute gas flows," *Microscale Thermophys. Eng.* **9**, 137 (2005).
- ³⁵N. G. Hadjiconstantinou, "Oscillatory shear-driven gas flows in the transition and free-molecular-flow regimes," *Phys. Fluids* **17**, 100611 (2005).
- ³⁶N. G. Hadjiconstantinou and H. A. Al-Mohssen, "A linearized kinetic formulation including a second-order slip model for an impulsive start problem at arbitrary Knudsen numbers," *J. Fluid Mech.* **533**, 47 (2005).
- ³⁷K. S. Breuer, "Lubrication in MEMS," in *Handbook of MEMS*, edited by M. Gad-el-Hak (CRC, Boca Raton, FL, 2002).
- ³⁸J. H. Park, P. Bahukudumbi, and A. Beskok, "Rarefaction effects on shear driven oscillatory gas flows: A direct simulation Monte Carlo study in the entire Knudsen regime," *Phys. Fluids* **16**, 317 (2004).
- ³⁹N. G. Hadjiconstantinou, "Sound wave propagation in transition-regime micro- and nanochannels," *Phys. Fluids* **14**, 802 (2002).
- ⁴⁰N. G. Hadjiconstantinou and O. Simek, "Sound propagation at small scales under continuum and non-continuum transport," *J. Fluid Mech.* **488**, 399 (2003).
- ⁴¹I. B. Crandall, *Theory of Vibrating Systems and Sound* (Van Nostrand, New York, 1926).
- ⁴²G. Kirchhoff, "Ueber den Einfluss der Wärmeleitung in einem Gase auf die Schallbewegung," *Ann. Phys. Chem.* **134**, 177 (1868).
- ⁴³J. W. S. Rayleigh, *The Theory of Sound* (Macmillan, New York, 1896), Vol. 2.
- ⁴⁴B. J. Hamrock, *Fundamentals of Fluid Film Lubrication* (McGraw-Hill, New York, 1994).
- ⁴⁵S. Fukui and R. Kaneko, "Analysis of ultra thin gas film lubrication based on linearized Boltzmann equation: First report-derivation of a generalized lubrication equation including thermal creep flow," *J. Tribol.* **110**, 253 (1988).
- ⁴⁶F. J. Alexander, A. L. Garcia, and B. J. Alder, "Direct simulation Monte Carlo for thin-film bearings," *Phys. Fluids* **6**, 3854 (1994).
- ⁴⁷L. Graetz, "On the thermal conduction of liquids," *Ann. Phys. Chem.* **25**, 337 (1885).
- ⁴⁸A. F. Mills, *Heat Transfer* (Irwin, Homewood, IL, 1992).
- ⁴⁹E. M. Sparrow and S. H. Lin, "Laminar heat transfer in tubes under slip flow conditions," *J. Heat Transfer* **84**, 363 (1962).
- ⁵⁰N. G. Hadjiconstantinou and O. Simek, "Constant-wall-temperature Nusselt number in micro and nano channels," *J. Heat Transfer* **124**, 356 (2002).
- ⁵¹N. G. Hadjiconstantinou, "Dissipation in small scale gaseous flows," *J. Heat Transfer* **125**, 944 (2003).
- ⁵²M. A. Gallis, D. J. Rader, and J. R. Torczynski, "Calculations of the

- near-wall thermophoretic force in rarefied gas flow,” *Phys. Fluids* **14**, 4290 (2002).
- ⁵³J. Tyndall, “On dust and disease,” *Proc. R. Inst. G. B.* **6**, 1 (1870).
- ⁵⁴M. A. Gallis, J. R. Torczynski, and D. J. Rader, “An approach for simulating the transport of spherical particles in a rarefied gas flow via the direct simulation Monte Carlo,” *Phys. Fluids* **13**, 3482 (2001).
- ⁵⁵H. S. Wijesinghe and N. G. Hadjiconstantinou, “A discussion of hybrid atomistic-continuum methods for multiscale hydrodynamics,” *Int. J. Multiscale Comp. Eng.* **2**, 189 (2004).
- ⁵⁶N. G. Hadjiconstantinou, “Discussion of recent developments in hybrid atomistic-continuum methods for multiscale hydrodynamics,” *Bull. Pol. Acad. Sci.: Tech. Sci.* **53**, 335 (2005).
- ⁵⁷W. Wagner, “A convergence proof for Bird’s direct simulation Monte Carlo method for the Boltzmann equation,” *J. Stat. Phys.* **66**, 1011 (1992).
- ⁵⁸F. J. Alexander, A. L. Garcia, and B. J. Alder, “A consistent Boltzmann algorithm,” *Phys. Rev. Lett.* **74**, 5212 (1995).
- ⁵⁹F. J. Alexander, A. L. Garcia, and B. J. Alder, “Cell size dependence of transport coefficients in stochastic particle algorithms,” *Phys. Fluids* **10**, 1540 (1998); erratum, *ibid.* **12**, 731 (2000).
- ⁶⁰N. G. Hadjiconstantinou, “Analysis of discretization in the direct simulation Monte Carlo,” *Phys. Fluids* **12**, 2634 (2000).
- ⁶¹D. J. Rader, M. A. Gallis, J. R. Torczynski, and W. Wagner, “DSMC convergence behavior of the hard-sphere-gas thermal conductivity for Fourier heat flow,” *Phys. Fluids* **18**, 077102 (2006).
- ⁶²A. L. Garcia and W. Wagner, “Time step truncation error in direct simulation Monte Carlo,” *Phys. Fluids* **12**, 2621 (2000).
- ⁶³N. G. Hadjiconstantinou, A. L. Garcia, M. Z. Bazant, and G. He, “Statistical error in particle simulations of hydrodynamic phenomena,” *J. Comput. Phys.* **187**, 274 (2003).
- ⁶⁴L. L. Baker and N. G. Hadjiconstantinou, “Variance reduction for Monte Carlo solutions of the Boltzmann equation,” *Phys. Fluids* **17**, 051703 (2005).
- ⁶⁵W. H. Press, S. A. Teukolsky, W. T. Vetterling, and B. P. Flannery, *Numerical Recipes in C* (Cambridge University Press, New York, 1994).
- ⁶⁶L. L. Baker and N. G. Hadjiconstantinou, “Variance reduction in particle methods for solving the Boltzmann equation,” in *Proceedings of the Fourth International Conference on Nanochannels, Microchannels and Minichannels*, Limerick, Ireland, 2006 (ASME, New York, 2006), paper ICNMM2006-96089.
- ⁶⁷R. G. Lord, “Some further extensions of the Cercignani-Lampis gas-surface interaction model,” *Phys. Fluids* **7**, 1159 (1995).
- ⁶⁸F. Sharipov, “Application of the Cercignani-Lampis scattering kernel to calculations of rarefied gas flows. I. Plane flow between two parallel plates,” *Eur. J. Mech. B/Fluids* **21**, 113 (2002).